ELSEVIER

Coordination Chemistry Reviews
177 (1998) 127–179

COORDINATION CHEMISTRY REVIEWS

Ligand-dependent excited state behaviour of Re(I) and Ru(II) carbonyl–diimine complexes

Derk J. Stufkens [a], Antonin Vlček Jr [b,*]

[a] *Anorganisch Chemisch Laboratorium, J.H. van't Hoff Research Institute, Universiteit van Amsterdam, Nieuwe Achtergracht 166, 1018 WV Amsterdam, The Netherlands*
[b] *Department of Chemistry, Queen Mary and Westfield College, London E1 4NS, UK*

Received 6 November 1997; accepted 20 April 1998

Contents

Abstract

The relations between the structure and excited state properties of $Re(E)(CO)_3(\alpha\text{-diimine})$ and $Ru(E)(E')(CO)_2(\alpha\text{-diimine})$ complexes (axial ligand E, E' = halide, alkyl, benzyl, metal fragment) are unravelled and discussed in detail. For example, it is shown how the increasing π-donor strength of an axial ligand, such as a halide changes the character of the lowest excited state from MLCT to LLCT. On the other hand, the presence of a covalently bound

* Corresponding author. Tel.: +44 171 7753260; fax: +44 181 9818745; e-mail: a.vleck@qmw.ac.uk

0010-8545/98/$ - see front matter
PII S0010-8545(98)00132-5

axial ligand in the coordination sphere introduces a $\sigma\pi^*$ lowest excited state that involves an excitation of an electron from the metal–ligand σ-bonding orbital to the π^* orbital of the α-diiamine. While the orbital parentage of the lowest excited state—MLCT, LLCT, $\sigma\pi^*$ or IL—is mostly determined by the axial ligand(s), its detailed properties (energy, lifetime, reactivity, decay mechanism) are dependent on both the axial and diimine ligands. Depending on the molecular structure and the medium, the excited state behaviour of these complexes ranges from a strong, long-lived emission to a very fast photochemical homolysis of a metal–ligand bond. Photochemical and photophysical properties of the complexes with different types of the lowest excited state are explored and pertinent structural effects discussed. It is shown how the excited state properties of the Re and Ru carbonyl–diimine complexes can be controlled by a judicious choice of the axial and diimine ligands and by the medium. These relations can be employed to design new functional molecular photonic materials, e.g. sensitisers, luminophores, photocatalysts, radical photoinitiators, luminescent probes or sensors.

Keywords: MLCT states; LLCT states; $\sigma\pi^*$ states; Photochemistry; Photophysics; Rhenium; Ruthenium; Diimine complexes

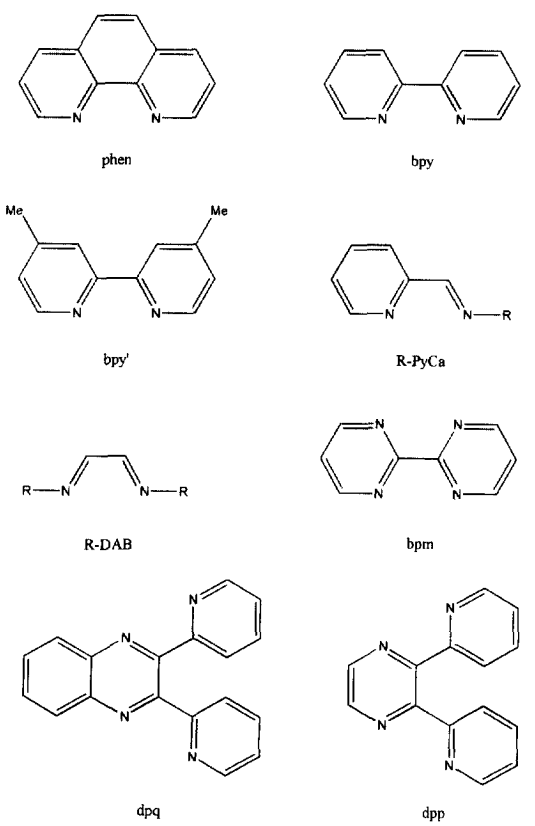

Scheme 1. Structural formulae of selected α-diimine and other acceptor ligands and the abbreviations used.

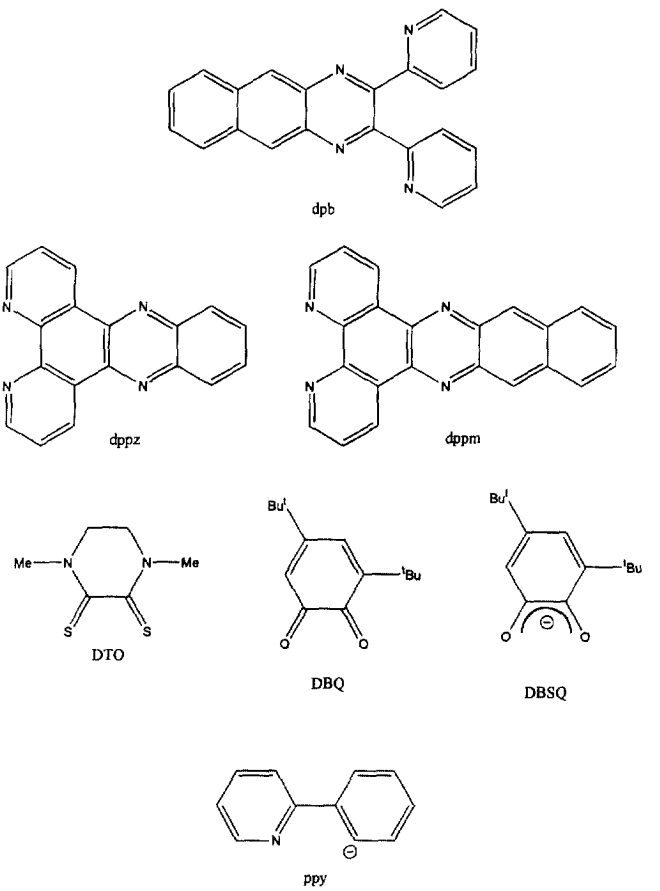

Scheme 1. (*Continued*)

1. Introduction

The spectroscopy, photochemistry and photophysics of Re(I) carbonyl–diimine complexes *fac*-Re(E)$(CO)_3(\alpha$-diimine$)^{0/+}$ (Fig. 1, left) continue to attract much research interest ever since their intriguing excited state properties were first recognised in the mid-1970s [1–4]. Depending on the nature of E and the diimine, these complexes are often strong luminophores, either in fluid solutions or in low-temperature glasses. Detailed studies of their emission have contributed to the development of theoretical models of the non-radiative deactivation of excited states and to the understanding of its mechanism [5–9]. The strong environmental sensitivity of the emission of Re(I) carbonyl–diimines has been employed to

monitor polymerisations [10], and to label [11,12] or photo-cleave [13] DNA or nucleobases [14]. Possible applications as luminescent sensors [15–18] or molecular materials for non-linear optics [19,20] or optical switching [21] are also emerging.

Most of the photochemistry of $Re(E)(CO)_3(\alpha\text{-diimine})^{0/+}$ complexes involves electron transfer. Early work has amply demonstrated that their excited states are both strong reductants and oxidants [2,4,22,23]. For example, excited $*[Re(Cl)(CO)_3(phen)]$ is oxidised to $[Re(Cl)(CO)_3(phen)]^+$ at -1.0 V versus SCE, while the reduction occurs at ca. $+1.0$ V, making this complex a very strong excited state oxidant [2]. Excited states of $Re(E)(CO)_3(\alpha\text{-diimine})^{0/+}$ complexes are often sufficiently long-lived (ns–μs) to become engaged in fast bimolecular electron or energy transfer reactions, similar to those of the famous family of $[Ru(bpy)_3]^{2+}$ and related polypyridyl complexes [24]. However, despite their higher stability towards photochemical ligand loss, the $Re(E)(CO)_3(\alpha\text{-diimine})^{0/+}$ complexes found less applications in light energy conversion schemes because of a limited stability [2,25–27] of their reduced or oxidised forms, which precludes their functioning as reversible redox photosensitisers. On the other hand, the high reactivity of the reduced species may be utilised in photocatalysis. For example, photoexcitation of $Re(Cl)(CO)_3(bpy)$, in the presence of a reductive quencher like triethanolamine, produces $[Re(Cl)(CO)_3(bpy)]^{-\cdot}$, which loses the Cl^- ligand. A further reaction with CO_2, present in the solution, results ultimately in the photocatalytic CO_2 reduction to CO via a rather complicated mechanism [28–34]. The $Re(E)(CO)_3(\alpha\text{-diimine})^{0/+}$ complexes also undergo very interesting intramolecular electron transfer reactions on excitation, provided that either the axial ligand E or the diimine bears a redox active substituent. Such reactions have provided a lot of information on the mechanism of intramolecular electron transfer [35–47] and on the dynamics of the fragmentation [48–52] or folding [18] of a ligand E upon its oxidation.

A completely different type of photoreactivity, a homolytic breaking of a Re–E bonds producing radicals, was observed recently for E = alkyl [53–61] or a metal fragment [3,62–75]. These reactions may find applications in photoinitiation of radical polymerisations. Obviously, the photochemical and photophysical behaviour of $Re(E)(CO)_3(\alpha\text{-diimine})^{0/+}$ complexes is strongly dependent on the composition of the coordination sphere, i.e. on the particular nature of the axial ligand E and the diimine, respectively. A great variety of these compounds may be synthesised since the nature of the axial ligand E can be varied broadly, ranging

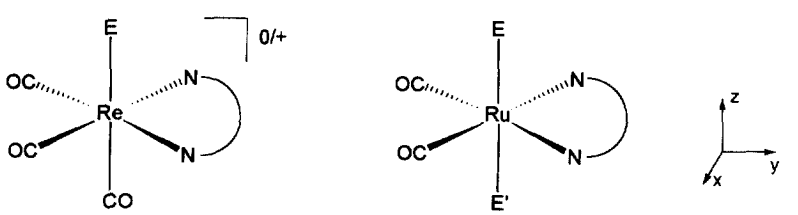

Fig. 1. Structures of the $Re(E)(CO)_3(\alpha\text{-diimine})^{0/+}$ and $Ru(E)(E')(CO)_2(\alpha\text{-diimine})$ complexes and chosen orientation of axes. (The Re complexes are neutral or cationic for anionic or neutral axial ligands E, respectively.)

from anionic ligands, like halides or CN^-, to neutral phosphines, pyridine derivatives, isonitriles, etc. Alkyls or metal-containing fragments like Ph_3Sn or $M(CO)_5$; (M = Re, Mn) were also employed as axial ligands. Extensive variations of the structure of the diimine ligand are possible as well.

The Ru carbonyl–diimine complexes of the type *trans,cis*-Ru(E)(E′)$(CO)_2$(α-diimine) (Fig. 1, right) form a new family of photoactive organometallic complexes [56,71,72,74–84]. Their excited state behaviour is qualitatively similar to that of their Re(E)$(CO)_3$(α-diimine)$^{0/+}$ counterparts. The Ru complexes are strongly emissive [72,74,77], their excited states undergo bimolecular electron or energy transfer reactions [77], and photochemical formation of radicals has been observed for E or E′ = alkyl [56,59] or a metal fragment [71,75,76]. These compounds afford even more structural flexibility than the Re complexes, since the ligands E and E′ may be varied to a large extent independently of each other. Thus, bis-halide, halide–alkyl, halide–metal, alkyl–metal or bis-metal complexes are known. Each of these classes exhibits a distinct spectroscopic, photochemical, photophysical or electrochemical behaviour.

From the above overview, it is evident that the strong dependence of photochemical and photophysical properties of Re(E)$(CO)_3$(α-diimine)$^{0/+}$ and Ru(E)(E′)$(CO)_2$(α-diimine) complexes on the axial ligand(s) E, E′ and the diimine, together with their great synthetic versatility, make these species very flexible photoactive materials that could be involved in various light-induced processes of both fundamental and applied interest. Their photobehavior reflects the structural dependence of the nature of their low-lying excited states. In principle, the presence of an electron-accepting α-diimine ligand in the coordination sphere allows for charge transfer, CT, electronic transitions directed to the diimine ligand, while the origin of the excited electron depends strongly on the actual complex composition, namely on the nature of the axial ligand(s). As will be shown in detail below, the photobehaviour of the Re(I) and Ru(II) carbonyl–diimine complexes may essentially be discussed in terms of four limiting types of excited states:

1. M → diimine metal-to-ligand charge transfer states, MLCT;
2. E → diimine ligand-to-ligand charge transfer states, LLCT (abbreviation XLCT is sometimes used for E = halide);
3. Transition from the M–E σ-bonding orbital to the diimine ligand, $\sigma\pi^*$;
4. Intraligand (diimine) $\pi\pi^*$ states, IL.

Ligand field (LF, also called metal-centred, MC, or dd) states appear to lie at rather high energies in the complexes discussed herein, thus being of a little photochemical importance.

Many new Re(E)(CO)(α-diimine)$^{0/+}$ and Ru(E)(E′)$(CO)_2$(α-diimine) complexes have recently been synthesised and pertinent spectroscopic, photophysical and photochemical data accumulated. Their analysis now allows us outline of general relationships between molecular structure and excited state behaviour of these Re(I) and Ru(II) carbonyl–diimine complexes, which will be discussed later.

2. Energy gap law as an indication of changing excited state character

Emission from $Re(E)(CO)_3(\alpha\text{-diimine})^{0/+}$ complexes often provides the first indication of the character of the low-lying excited state(s). The shape of the emission band, its maximum energy E_{em}, quantum yield ϕ_{em}, lifetime τ, and the half-width of the emission band at full maximum $\Delta\tilde{\nu}_{1/2}$, are the directly measurable experimental data. The rate constants of the radiative and non-radiative decay, k_r and k_{nr}, respectively, may easily be calculated from the experimentally available quantities: $\tau = 1/(k_r + k_{nr})$; $\phi_{em} = k_r/(k_r + k_{nr})$, assuming that the emitting excited state is populated with an efficiency of unity. In most of the complexes discussed herein, the excited state deactivation is dominated by the non-radiative mechanism: $k_{nr} \gg k_r$ and, hence, $\tau \cong 1/k_{nr}$.

The radiative rate constant is approximately proportional [9,85] to the cube of the emission energy and to the square of the transition moment:

$$k_r \propto E_{em}^3 \langle \Psi_e | \tilde{\mu} | \Psi_g \rangle^2, \tag{1}$$

where Ψ_e and Ψ_g are the wave functions of the excited and ground state, respectively, and $\tilde{\mu}$ is the dipole moment operator. However, the linear dependence of k_r on E_{em}^3 is seldom followed accurately, even in series of structurally related complexes, apparently because of a large structure-sensitivity of the transition moment.

Rate constants of the non-radiative deactivation of excited $Re(E)(CO)_3(\alpha\text{-diimine})^{0/+}$ complexes often exhibit Arrhenius-like temperature dependence [8,86] described by Eq. (2) or Eq. (3):

$$k_{nr} = k_0 + A \exp\left(\frac{-E_a}{k_B T}\right), \tag{2}$$

$$k_{nr} = \frac{k_0 + A \exp\left(\frac{-E_a}{k_B T}\right)}{1 + \exp\left(\frac{-E_a}{k_B T}\right)}, \tag{3}$$

in which k_0 represents the rate of the non-radiative deactivation of the excited state by weak coupling to the ground state. The exponential term stands for a deactivation via a higher lying excited state that decays very rapidly, either with or without a net chemical change. E_a is an apparent activation energy needed to populate the higher lying state, i.e. the energy difference between the crossing point of the potential energy surfaces of the two excited states in question and the zero-level energy of the initial (emissive) excited state. k_B is the Boltzmann constant. Eq. (3) is more appropriate if the two excited states are in a thermal equilibrium and their energy difference is small: $E_a < k_B T$. More complicated versions of Eq. (3) have to be used if more than one higher state is involved in the deactivation process [86]. For the complexes studied herein, the thermally activated deactivation pathway becomes relatively unimportant at low temperatures (77 K) at which the excited state decay is dominated by the weak coupling to the ground state: $k_{nr} \cong k_0 \cong 1/\tau$.

This is the case of virtually all the Re and Ru carbonyl–diimine complexes discussed herein. The weak coupling mechanism is usually the most important deactivation pathway, even at ambient temperatures.

Theoretical treatment of the temperature-independent decay pathway k_0 within the low-temperature limit of the weak vibrational coupling model [5,6,8,9,37,85,87–89] leads to the energy gap law (EGL). Briefly, the excited and ground states are vibronically coupled by a promoting vibration(s) k of frequency ω_k and/or by spin–orbit interaction. Promoting vibrations remove the orthogonality of the states Ψ_e and Ψ_g and thus allows for the non-radiative transition to take place. They induce changes in the ground and excited state overlap, bringing the excited electron and the hole together. At the same time, an admixture with an intermediate spin-singlet state via a spin–orbit coupling mechanism would remove spin restrictions on the non-radiative decay. A non-radiative transition is assumed to occur from the lowest vibrational level of the electronically excited state Ψ_e into isoenergetic, highly excited vibrational levels of the electronic ground state Ψ_g. The excited state energy is thus converted into the energy of the ground state acceptor vibrations i of angular frequency ω_i. (Note that the acceptor vibrations are different from the promoting ones.) Acceptor vibrations correspond to those normal coordinates Q_i which are displaced upon the electronic excitation, i.e. to the vibrations of those bonds whose lengths and/or angles are changed by the electronic excitation. Excited state displacement of a normal coordinate Q_i is described by a dimensionless parameter $\Delta_i = (M_i\omega_i/\hbar)^{1/2}\Delta Q_i$, where ΔQ_i is the actual difference in the normal coordinate i between the excited and ground state and M_i is the reduced mass. For practical reasons, a single acceptor vibration m of a mean frequency ω_m and a mean displacement parameter $\Delta_m^2 = \Sigma\Delta_i^2$, which describes the overall excited state distortion, are used instead of individual ω_i and Δ_i values.

The former is defined as a weighted average of the frequencies of individual acceptor vibrations i: $\hbar\omega_m = \hbar\Sigma\Delta_i^2\omega_i^2/\Sigma\Delta_i^2\omega_i$. Notably, the acceptor vibrations give rise to the vibrational structure of emission bands and to resonance enhanced Raman peaks. Hence, they may be identified and their relative importance assessed independently by spectroscopic experiments.

Quantitatively, the model of a weak vibrational coupling between the excited and ground state is applicable whenever the energy difference between the ground and excited state ΔE is much larger than the electron–vibrational coupling: $\Delta E \gg S_m\hbar\omega_m$. The electron–vibrational coupling constant (the Huang–Rhys factor) S_m is related to the excited state distortion: $S_m = \Delta_m^2/2 = \Sigma\Delta_i^2/2$. (Note that $\hbar\omega_m\Delta_m^2$ is the emission Stokes shift.) The excited state energy ΔE is usually approximated by the emission energy E_{em}. The high-frequency acceptor vibrations m are treated within the low-temperature limit, $\hbar\omega_m \gg k_B T$, while the low-frequency intramolecular and solvent vibrations are treated classically. They are described collectively by the parameter χ_0 which is related to the half-width of the emission band.

Theoretical treatment of this situation [9,85,87,88] predicts an exponential decrease of k_0 with increasing ΔE: $k_0 \propto \exp(-\gamma\Delta E/\hbar\omega_m)$, as well as the dependence of k_0 on the excited state distortion and mean acceptor frequency:

$$\ln k_0 = \ln \beta - \frac{1}{2} \ln \hbar\omega_m E_{em} - S_m - \frac{\gamma E_{em}}{\hbar\omega_m} + \chi_0 k_B T \left(\frac{\gamma + 1}{\hbar\omega_m} \right)^2, \quad (4)$$

$$\gamma = \ln \left(\frac{E_{em}}{\hbar\omega_m S_m} \right) - 1. \quad (5)$$

The parameter β describes the electronic coupling between the two states. Generally [87,88,90], it is a product of the spin–orbit coupling integrals H_{so} and terms describing the vibronic coupling between the excited and ground states through the promoting vibration(s) ω_k:

$$\beta \propto H_{so} \cdot C^2 \omega_k \sqrt{\pi/2}, \quad (6)$$

$$C^2 = \frac{\hbar^2}{M_k} \left\langle \Psi_g \left| i \frac{\partial}{\partial Q_k} \right| \Psi_e \right\rangle^2. \quad (7)$$

Despite several approximations [9], Eq. (4) is a very convenient basis for the discussion of structural effects on the non-radiative decay rate. The dependence of both γ and $\ln \beta$ on E_{em} is rather weak. Hence, for a series of structurally related emissive compounds, Eq. (4) predicts that $\ln k_0$ will decrease (and hence $\ln \tau$ will increase) linearly with increasing emission energy E_{em}. Moreover, it follows that the rate of non-radiative decay will decrease with decreasing excited state distortion S_m, diminishing electronic coupling, and with decreasing role of the low-frequency skeletal and solvent vibrations in accepting the excited state energy, χ_0. The acceptor frequency $\hbar\omega_m$ determines the slope of the $\ln k_0 - E_{em}$ correlations, $-\gamma/\hbar\omega_m$. Hence, the sensitivity of the decay rate to the emission energy will increase with decreasing acceptor frequency. These predictions of the weak coupling model account for many aspects of excited state behaviour and may also be used to design molecules with excited states of predetermined properties [89,91] (see Section 4.1).

The linear correlation between the logarithm of the non-radiative decay rate and the emission energy is usually called the EGL. It is expected to hold for any series of compounds that meet the following requirements:

1. Excited state decays through the same acceptor vibrations of similar frequencies.
2. The vibronic coupling term $C^2\omega_k$ and the spin–orbit interaction do not appreciably vary within the series.
3. The factor S_m does not change significantly, i.e. the excited state distortions of individual species are comparable. In fact, it has been shown [8] that S_m may increase linearly with increasing E_{em}, not affecting the linearity of the $\ln k_0 - E_{em}$ correlation.
4. No large changes in solvation occur.

The set of conditions (1)–(4) can be met only in a series of such compounds that are structurally closely similar and share an excited state of a common orbital origin. The validity of the EGL has been tested for numerous series of coordination compounds with excited states of different orbital parentage. Linear correlations between $\ln k_{nr}$ and E_{em} were observed for the emission from LF states of $[Rh(NH_3)_5L]^{3+}$ complexes [6], for $d\sigma^*p\sigma$ emission from $[Rh_2(CNR)_4(L)_2]^{2+}$ dimers [6], emission from MLCT states of several series of polypyridyl complexes [5,9,85],

namely $[Os^{II}(phen)_2(L)_2]^{2+}$, $[Os^{II}(bpy)_2(L)_2]^{2+}$ or $[Ru^{II}(phen)_2(L)_2]^{2+}$. Very good linear EGL correlations were found for each of these classes of compounds. The slopes and intercepts are, expectedly, different for each class.

As for the $Re(E)(CO)_3(\alpha\text{-diimine})^{n+}$ complexes, good EGL correlations were found [6,92–95] for the MLCT emission from an extensive series of complexes containing the same α-diimine ligand while the axial ligand E was varied: $n = 0$, $L = Cl$; $n = 1$, $L = CH_3CN$, PMe_3, pyridine derivatives, *N*-methylimidazole, etc. Alternatively, good EGL correlations were obtained by changing the substituents on the bpy ligand [8,78,94]. Large changes in the diimine structure lead to deviations from EGL behaviour and, generally, each diimine ligand gives rise to a separate EGL correlation for the corresponding $Re(E)(CO)_3(\alpha\text{-diimine})^{n+}$ series [5,93] (see Section 4.1 and Fig. 19). In several cases, the observed non-radiative decay rates were quantitatively well-reproduced using S_m and ω_m parameters obtained from the analysis of the shape of emission bands and/or rR spectra [8,47,93]. It followed that the intraligand (diimine) vibrations are the most effective acceptor modes. Stretching ν(CO) vibrations are also involved in the deactivation of the excited states of carbonyl–diimine complexes, but their relative contribution appears to be less important [8,93]. A large width of the emission bands suggests an important acceptor role of the low-frequency skeletal and especially, solvent vibrations. For example, values of $\hbar\omega_m$ (1450 cm^{-1}) and χ_0 (1100 cm^{-1} in EtOH:MeOH (4:1 v/v) and 650 cm^{-1} in 2Me–THF) were obtained [8] for the $Re(Cl)(CO)_3(4,4'\text{-}X_2\text{-bpy})$ series. Notably, the $\hbar\omega_m$ value of 1450 cm^{-1} is significantly larger than that found for Ru and Os bipyridine complexes, 1350 cm^{-1}, which do not contain any CO ligand. This was attributed to the involvement of the high-frequency ν(CO) vibration at approximately 2020 cm^{-1} as one of the acceptor vibrations for the Re species. Values of χ_0 are also much larger than those found for Os or Ru polypyridine complexes. The combination of a large solvation reorganisation energy and activation of skeletal vibrations is also responsible for relatively large Stokes shifts and broadening of the emission bands which precludes observation of vibronic structures for the MLCT emission of $Re(E)(CO)_3(\alpha\text{-diimine})^{0/+}$ complexes.

The examples discussed above show clearly that EGL serves as a general basis for the understanding of the nonradiative excited state decay. Linear EGL correlations are observed in series of structurally related compounds which share an emitting excited state of a common character, namely of the same orbital parentage. Sudden changes in EGL correlations usually indicate a changing excited state character. 'EGL maps', i.e. plots of $\ln k_0$ (or simply $-\ln \tau$) versus E_{em} for a family of compounds investigated, thus provide a good insight into ligand effects on the excited state character. Figs. 2 and 3 show such EGL maps for the newly investigated Re(I) and Ru(II) complexes containing halide, alkyl, or metal-coordinated ligands.

Even a brief perusal of these maps shows that the complexes can be grouped into two different families with profoundly different characters of their emitting excited state: the halide containing complexes and those with Re–metal or Ru–metal bonds, respectively. Each of them is characterised by a distinct EGL correlation.

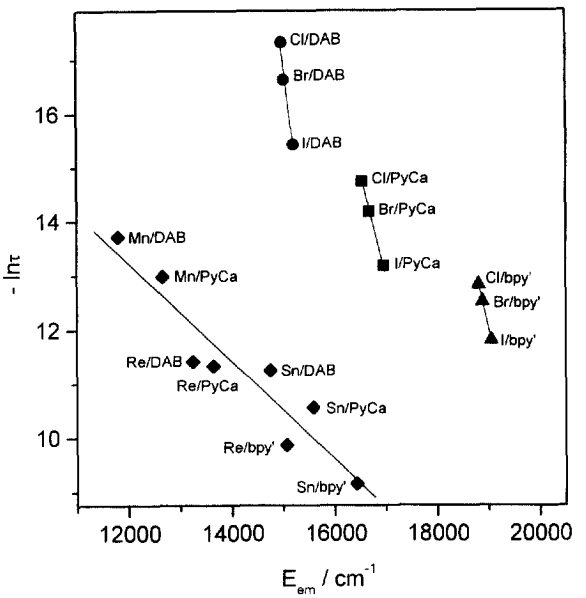

Fig. 2. EGL map of $Re(E)(CO)_3(\alpha\text{-diimine})$ complexes. Values of the emission energies E_{em} and lifetimes τ were obtained in 2Me–THF glasses at 80 K to avoid any influence of the thermally activated decay pathway: $k_{nr} \cong k_0$. The rate of radiative decay is negligible; $k_r \ll k_{nr}$. Hence, $1/\tau \cong k_{nr} \cong k_0$, where k_0 is the rate constant of the non-radiative decay of the excited state to the ground state by the weak coupling mechanism. The dependence of $-\ln \tau$ on E_{em} is thus equivalent to the EGL correlation, $\ln k_0$ vs. E_{em}, see Eq. (4). Data from Refs. [53,60,62,73,112].

Closer inspection of the halide complexes suggests that another change in the excited state character occurs when the halide ligand changes from Cl to Br and I since the strong drop of $\ln k_0$ is not accompanied by any significant decrease of E_{em}. A comparison of Figs. 2 and 3 also shows that variations in the ligand character has qualitatively similar effects on both the Re and Ru species. Using these EGL maps as a starting point, the ligand dependence of the character of the low-lying excited states will now be explored in more detail.

3. Effects of the axial ligands

3.1. Complexes with lowest Re, Ru → diimine MLCT excited states

Most of the cationic complexes $Re(E)(CO)_3(\alpha\text{-diimine})^+$ and neutral $Re(Cl)(CO)_3(\alpha\text{-diimine})$ species studied so far exhibit a spectroscopic, photophysical and photochemical behaviour that was attributed to (Re → diimine) MLCT excited states. Axial ligands E are π-acceptors, π-neutral ligands or very weak π-donors. Complexes of this type are known for E = pyridine derivatives, nitriles [96], isonitriles [16], phosphines [32,97], phosphites [97], acetylenes [98,99], histidine

[100], imidazole [23], 9-ethylguanine nucleobase [14], and binuclear complexes [43,101–108] in which the axial ligand (bis-pyridine derivative or CN^-) forms a bridge to another metal atom. Derivatives of bpy, phen and other polypyridyls are the most commonly used diimines. Increasing attention is being paid to complexes with PyCa and DAB-type ligands. Lowest MLCT excited state was also well established [76–78] for $Ru(Cl)(R)(CO)_2(\alpha\text{-diimine})$ complexes; R = alkyl.

In general, complexes with lowest MLCT states display a rather intense (2000–6000 M^{-1} cm^{-1}) absorption band in the visible spectral region which shifts to lower energies (longer wavelengths) with decreasing solvent polarity due to a characteristic solvatochromism [4,46,109,110]. This is indicative of a significant change in the charge distribution on MLCT excitation. Emission bands of these complexes are broad, structureless, and exhibit a rigidochromic effect, i.e. a shift to higher energy on going from a fluid to glassy solution [46,110]. Emission lifetimes are EGL-controlled [6,8,78,93–95]. Low-temperature (4–77 K) emission studies of $Re(Cl)(CO)_3(diimine)$ complexes; (diimine = phen, bpy, bpy'); have revealed [7] that the emitting state is split by a second order spin–orbit coupling into three spin sublevels. However, the overall splitting is small, less than 100 cm^{-1}. Hence, the emitting state is adequately described as a spin-triplet, ^{3}MLCT, the spin–orbit splitting playing no significant role in the experiments carried out at or above 77 K, despite the presence of the heavy Re atom.

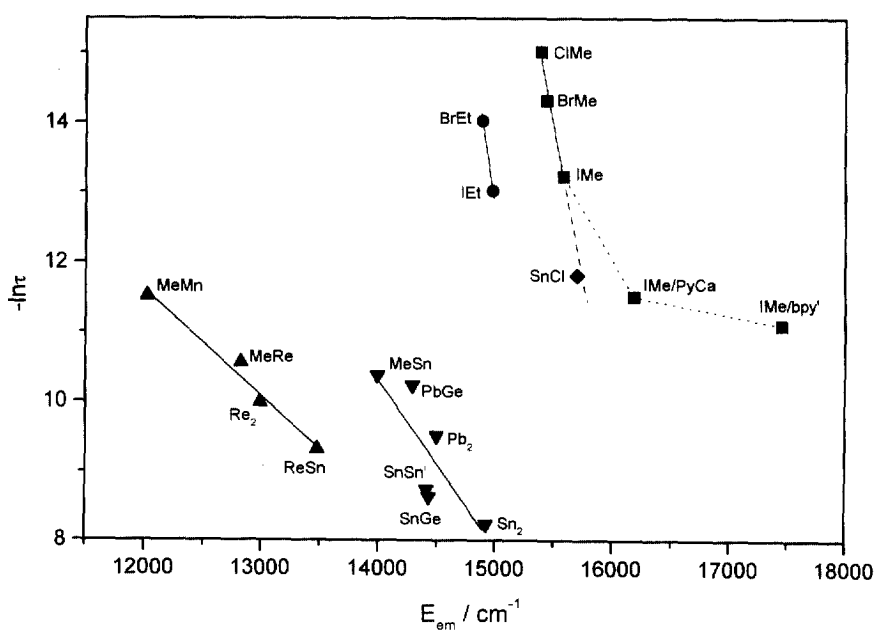

Fig. 3. EGL map of $Ru(E)(E')(CO)_2(\alpha\text{-diimine})$ complexes. Conditions as in Fig. 2. Data from Refs. [72,74,77].

MLCT excited states of the Re or Ru carbonyl–diimine complexes may be simply viewed as charge-separated species $*[Re^{II}(E)(CO)_3(\alpha\text{-diimine}^{\bullet -})]^{0/+}$ or $*[Ru^{III}(Cl)(E')(CO)_2(\alpha\text{-diimine}^{\bullet -})]$, respectively. Such a charge separation has unmistakable spectroscopic signatures. Thus, time-resolved UV–vis absorption spectra of ^{3}MLCT-excited Re(Cl)(CO)$_3$(α-diimine) complexes, diimine = bpy or phen derivatives [22] or of Re(X)(CO)$_3$(bpy′) (X = Cl, Br) [111,112] are rather similar to the spectra of the corresponding reduced Re(Cl)(CO)$_3$(α-diimine)$^{\bullet -}$ species, which in turn resemble spectra of the radical-anions of the free ligands. These observations point to the presence of a diimine$^{\bullet -}$ chromophore in ^{3}MLCT excited states. The virtual reduction of the diimine ligand in MLCT excited state is directly evidenced by time-resolved resonance Raman (TR^3) spectra that reveal a shift of the symmetrical stretching vibration of the two diimine C=N bonds, ν_s(CN), to lower frequencies on excitation. For example, the TR^3 spectrum of [Ru(Cl)(Me)(CO)$_2$(*i*Pr-DAB)] showed a shift of the ν_s(CN) band from 1569 to 1486 cm^{-1} on MLCT excitation [78], while the TR^3 spectrum of MLCT-excited $*[Re(4\text{-Etpy})(CO)_3(bpy)]^+$ displays a typical spectral pattern of bpy$^{\bullet -}$ [39]. Accordingly, ground state Raman spectra show strong resonance enhancement of the peak due to the ν_s(CN) vibration when measured with excitation tuned into the MLCT absorption band [8,72,76,81,112–114].

Virtual oxidation of the metal atom in the MLCT excited state decreases the M→CO π-back bonding, thus strengthening (shortening) the C≡O bonds. This excited state distortion manifests itself by the resonance enhancement of the Raman band belonging to the in-phase ν_s(CO) stretching vibration when the Raman spectrum is measured using excitation within the MLCT absorption band [8,72,76,81,112–116]. The structural effect of the MLCT excitation on the CO ligands may be followed quantitatively using time-resolved IR spectroscopy of the ^{3}MLCT excited state. Indeed, significant shifts of the ν(CO) IR bands to higher frequencies were observed on going from the ground to ^{3}MLCT states. Thus, the pump-probe nanosecond time-resolved IR spectrum of Re(Cl)(CO)$_3$(bpy) shows [117] an average shift of the three ν(CO) bands by + 55 cm^{-1} on MLCT excitation while a shift by + 46 cm^{-1} was observed in a step-scan TR-FTIR spectrum of $*[Re(4\text{-Mepy})(CO)_3(phen)]^+$ measured 600 ns after excitation [118], clearly indicating the MLCT character of the excited state. Resonance enhancement of ν(CO) Raman peaks and large high-frequency shifts of ν(CO) IR bands are thus good experimental criteria for the MLCT character of the lowest excited state in carbonyl–diimine complexes.

The temperature dependence of the non-radiative decay of a typical MLCT state of Re(Cl)(CO)$_3$(bpy) is satisfactorily described by Eq. (3) with the following parameters: $A = 4.9 \times 10^7$ s^{-1}, $E_a = 270$ cm^{-1} in 2-Me–THF solution [8]. These parameters are close to those found [86] for $[Os(bpy)_3]^{2+}$ ($k_0 = 3.7 \times 10^6$ s^{-1}, $A = 7.2 \times 10^7$ s^{-1}, $E_a = 312$ cm^{-1}). A larger activation energy of 1130 cm^{-1} ($k_0 = 3.4 \times 10^6$ s^{-1}, $A = 1.8 \times 10^8$ s^{-1}) was measured [8] for [Re(4-Etpy)-(CO)$_3$(bpy)]$^+$. The nature of the higher excited state involved in the thermal deactivation is yet unclear. It may be another spin- or orbital-component of the manifold of MLCT states that originates in excitations from the three nondegener-

ate d_π orbitals. The photochemical stability excludes the possibility of a thermal population of a LF state. Moreover, the A values found for all the Re and Ru carbonyl–diimine complexes studied are much smaller than those observed for the thermally activated MLCT → LF transition in the case of $[Ru(bpy)_3]^{2+}$ and related Ru^{II} polypyridyl complexes: 10^{13}–10^{14} s^{-1}. The (Re → 4-Etpy) MLCT state may be involved in the thermally activated decay of $[Re(4\text{-}Etpy)(CO)_3(bpy)]^+$.

Variations in the axial ligand E influence the MLCT excited state lifetime of $Re(E)(CO)_3(\alpha\text{-diimine})^{0/+}$ complexes according to the EGL. Thus, increasing the π-acceptor strength of the axial ligand E shifts both the MLCT absorption and emission to higher energies (shorter wavelengths) due to stabilisation of the Re-d_π orbitals. Hence, the excited state lifetime increases because of a decrease in the rate of the non-radiative deactivation, according to EGL. At the same time, the emission quantum yields increase, because of an increase of k_r with E^3_{em} and a decrease of k_{nr}. This becomes especially apparent in the case of cationic complexes with E = PPh_3, CH_3CN, or isonitriles, for which ϕ_{em} reaches values of 0.4–0.8 and room temperature lifetimes are in the microsecond range [6,16]. However, the rise in the MLCT excited state energies for π-accepting axial ligands also diminishes the energy difference between the MLCT state and higher lying IL states whose energies are much less sensitive to the chemical nature of the axial ligand. Hence, a change in the character of the lowest excited state from MLCT to IL may occur on introducing strongly π-accepting axial ligands, see Section 4.2. This is the case of, for example, the $Re(CO)_4(bpy)^+$ and $Re(CO)_4(phen)^+$ complexes [119–122].

Re(I) and Ru(II) carbonyl–diimine complexes with the MLCT lowest excited state do not undergo any ligand photodissociation under visible light irradiation, except for the $Ru(I)(Me)(CO)_2(bpy')$ complex, which shows a CO photodissociation [123]. Bimolecular energy and electron transfer reactions of long-lived MLCT excited states are commonplace for both the Re [2,22] and Ru [77] species. Their rates and energetics are affected by the nature of the axial or diimine ligand through their effects on the excited state reduction and oxidation potentials and lifetimes.

3.2. Intramolecular reduction of the axial ligand and (Re → E) MLCT excited states

An interesting intramolecular photoreactivity occurs when the axial ligand is itself reducible or if it bears a reducible substituent. An electron-accepting axial ligand introduces a (Re → E) MLCT state which may be populated either by a $bpy^{\cdot -}$ → E intramolecular electron transfer from the (Re → bpy) MLCT state: $[Re^{II}(E)(CO)_3(bpy^{\cdot -})] \rightarrow [Re^{II}(E^{\cdot -})(CO)_3(bpy)]$, or by a direct, usually weak, (Re → E) MLCT transition [36,41,47,124], see Fig. 4. The intramolecular electron transfer actually amounts to a non-radiative transition between two different MLCT excited states. For E = *N*-methyl-4,4′-bipyridinium, MQ^+, it is fully completed in 7 ns [41], i.e. $k_{et} \gg 1.4 \times 10^8$ s^{-1}. Slower rates were measured for axial ligands in which the acceptor group is separated from the coordinating pyridine fragment by a spacer [42]. The (Re → MQ^+) MLCT excited state was characterised by a time-resolved

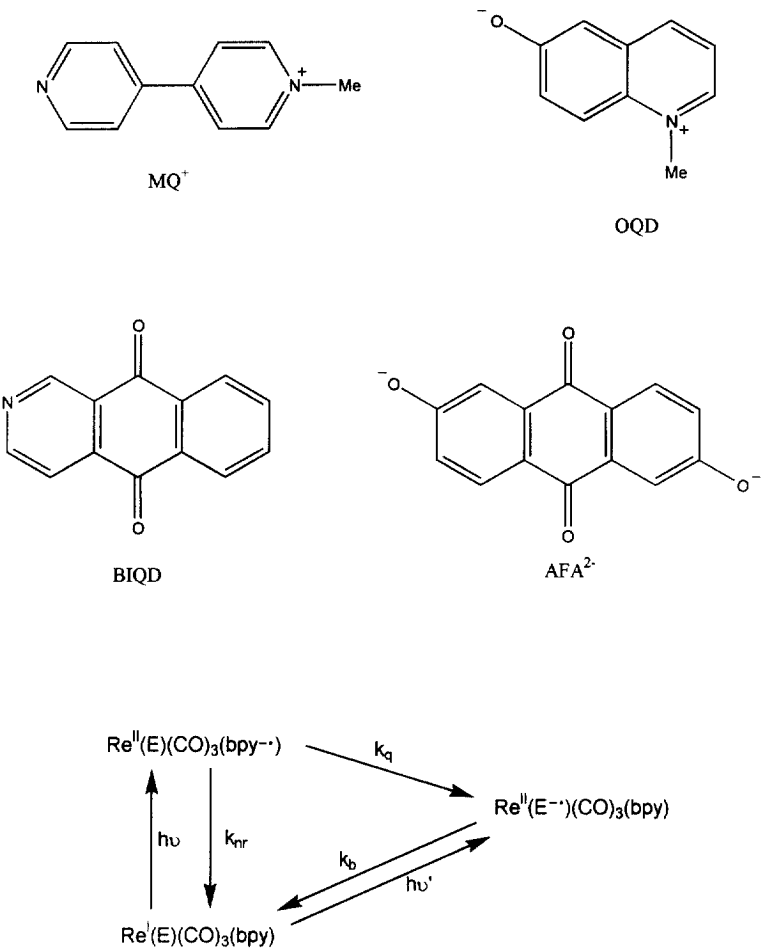

Fig. 4. Top: structures of some of the reducible axial ligands known to give rise to Re→E MLCT excited states of Re complexes. Bottom: mechanism of the population of (Re→E) MLCT states in complexes with reducible axial ligands E. *hν* and *hν'* denote the (Re→bpy) and (Re→E) MLCT optical excitations, respectively. k_q corresponds to the bpy$^{\cdot -}$→E intramolecular electron transfer from the (Re→bpy) MLCT excited state. k_0 and k_b are the non-radiative decay rate constants of the (Re→bpy) and (Re→E) MLCT excited states, respectively. The (Re→E) MLCT states may also decay radiatively. Values for $[Re(MQ^+)(CO)_3(bpy)]^{2+}$: $k_q > 2 \times 10^8\ s^{-1}$, $k_b = 5 \times 10^7\ s^{-1}$, $k_{nr} = 4.5 \times 10^6\ s^{-1}$ [41].

resonance Ramon spectrum that shows peaks of the reduced MQ$^{\cdot}$ radical [41]. A pyridine molecule with attached crown-ether ring that incorporates an oxidising nitrobenzene group [17,18] represents another interesting type of axial redox-active ligands. The intramolecular electron transfer from the (Re→bpy) MLCT state to the nitrobenzene unit triggers folding of the crown-ether link [18]. Complexes in which an oxidising axial ligand BIQD, AFA^{2-}, or OQD (see Fig. 4) is directly coordinated to the Re atom exhibit [47] a weak absorption band due to the

(Re → E) MLCT transition in the visible spectral region. The (Re → E) ^{3}MLCT state is the lowest excited state and the origin of the emission. Experimentally measured rates of the non-radiative decay of (Re → E) ^{3}MLCT excited states (i.e. of an $E^{\bullet -} \rightarrow Re^{II}$ electron transfer) were well reproduced by EGL calculations using parameters derived from the analysis of the corresponding emission bands [47]. Interestingly, the rate constants are rather small (4×10^7, 1.3×10^5 and 6.6×10^4 s^{-1} for E = BIQD, AFA^{2-} and OQD, respectively) despite a direct bond between the redox active ligand and the Re atom. This appears to be caused by a small electronic coupling.

Many dinuclear or oligonuclear complexes $[Re(CO)_3(\alpha\text{-diimine})(\mu\text{-E})ML_n)]^{n+}$ are known in which the axial ligand forms a bridge to another metal centre. Bridging ligands such as 4,4′-bpy, α,ω-bis-pyridine-alkanes, pyrazine, CN^-, etc., were used. Depending on the nature of the bridging ligand, the lowest excited state of the Re moiety is either (Re → diimine) or (Re → E) MLCT in character. Excitation into either of these MLCT transitions gives rise to a wide variety of intramolecular processes that originate in the MLCT-excited {Re(α-diimine)$(CO)_3$} fragment. For example, energy transfer (e.g. for $ML_n = Ru^{II}(bpy)_2(L)^{2+}$), reduction or oxidation of the ML_n group (e.g. $Ru^{III}(NH_3)_5^{3+}$ or $Ru^{II}(NH_3)_5^{2+}$, respectively) were observed [43,101–108,125]. These processes are amply investigated as a part of the quest for broad-band light absorbing ('antenna') supramolecular systems and sensitisers [125,126]. Their detailed discussion is outside the scope of this review.

3.3. (E → diimine) LLCT excited states derived from reducing axial ligands

An intramolecular $E \rightarrow Re^{II}$ electron transfer occurs from (Re → bpy) MLCT states of those complexes that contain an axial ligand E that bears a reducing group. For example, this is the case of the py-PTZ complexes [35,37–39,45,46,127], see Fig. 5. Optical excitation of $[Re^{I}(py\text{-}PTZ)(CO)_3(bpy)]^-$ first populates the $[Re^{II}(py\text{-}PTZ)(CO)_3(bpy^{\bullet -})]^+$ MLCT excited state. Then, an electron is transferred from py-PTZ to Re^{II} with a rate constant of 4.8×10^9 s^{-1} or faster [35]. The species produced, $[Re^{I}(py\text{-}PTZ^{\bullet +})(CO)_3(bpy^{\bullet -})]^+$ may be viewed as a py-PTZ → diimine ligand to ligand charge transfer, LLCT, excited state. It was identified by time-resolved resonance Raman and UV–vis absorption spectroscopies that showed features characteristic of the reduced $bpy^{\bullet -}$ and oxidised $PTZ^{\bullet +}$ moieties [35,39,127]. This LLCT state decays to the ground state by another intramolecular electron transfer, $bpy^{\bullet -} \rightarrow py\text{-}PTZ^{\bullet -}$. This is a highly exergonic step, $\Delta G^0 \cong -2$ eV, which occurs in the inverted region [37]. The rate constant of the non-radiative decay of the LLCT state depends on ΔG^0 according to EGL [37]. Actual values measured for the $[Re^{I}(py\text{-}PTZ)(CO)_3(\alpha\text{-diimine})]^+$ (diimine = 4,4′-X_2-bpy or 2,2′-bipyrazine) species vary in the range from 6.7×10^6 to 9.1×10^7 s^{-1} [37]. The (py-PTZ → diimine) LLCT electronic transition was observed in the absorption spectra of $[Re^{I}(py\text{-}PTZ)(CO)_3(\alpha\text{-diimine})]^+$ complexes, diimine 4,4′-Me_2-bpy, 4,4′-$(MeO)_2$-bpy or Me_4-phen. It is manifested as an extremely weak ($\epsilon = 2.4$ M^{-1} s^{-1}) shoulder on the low-energy onset of the MLCT absorption band [40]. Analysis of the shape of this weak shoulder provided the value for the electronic coupling term

between the LLCT state and the ground state, e.g. 44 cm^{-1} for bpy′. This value agrees well with that derived from the EGL correlation between the rate constant of the non-radiative decay of the LLCT state and the driving force ΔG^0 [37]. The spectral weakness of the (py-PTZ → diimine) LLCT transition is fully understandable, given the weak electronic interaction between the diimine and the PTZ moieties due to their long distance and unfavourable mutual orientation.

In a related study [44,45], the reducing 4-*N*,*N*-diaminobenzoyl group (DMAB) was linked to the axial pyridine ligand in $[Re(py\text{-}DMAB)(CO)_3(bpy)]^+$ through a peptide spacer of variable length that consisted of several proline residua. The kinetics of the DMAB → Re^{II} intramolecular electron transfer from the MLCT state was measured and found to decrease from 9.8×10^7 to 5.3×10^6 and to 5.6×10^5 s^{-1} when the number of proline residua in the spacer increased from 0 to 1 and to 2, respectively. Conformational effects of the oligoproline spacer on the rate of the long-range electron transfer were revealed by the temperature dependence of the rate of the electron transfer.

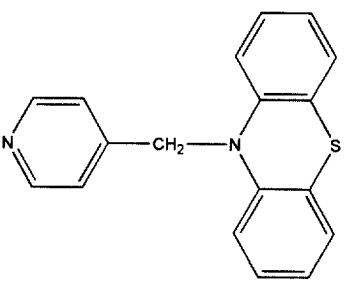

py-PTZ

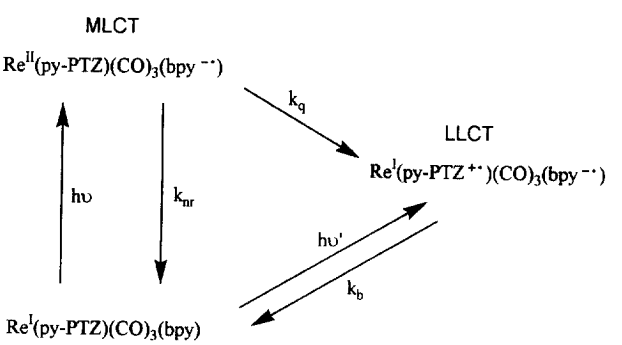

Fig. 5. Structure of the oxidisable py-PTZ ligand and mechanism of the population of the (py-PTZ → bpy) LLCT state for $[Re(py\text{-}PTZ)(CO)_3(bpy)]^+$: $k_q > 2 \times 10^8$ s^{-1}, $k_b = 1.1 \times 10^7$ s^{-1} [37]. The direct optical transition to the LLCT state, *hν′*, is extremely weak, see text.

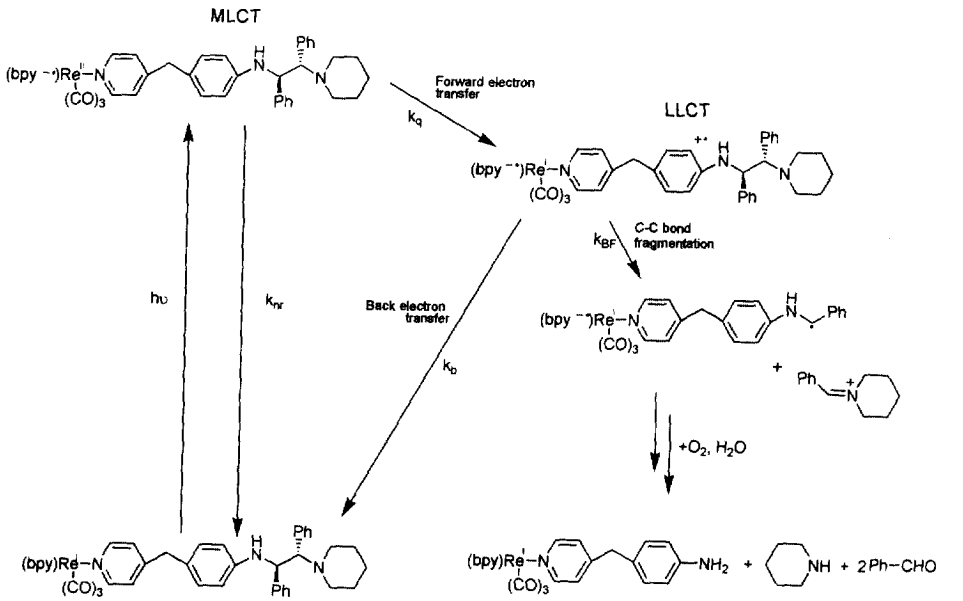

Fig. 6. The C–C bond fragmentation of the 1,2-diamine-1,2-phenyl-ethyl group of the axial ligand E, triggered by the population of a (E → bpy) LLCT state in air-saturated CH_3CN solution. $k_b = 1 \times 10^8$ s^{-1}, $k_{BF} = 3 \times 10^8$ s^{-1} [49].

An irreversible intramolecular photochemistry occurs from (E → diimine) LLCT excited states of those $[Re(E)(CO)_3(\alpha\text{-diimine})]^+$ complexes whose axial ligand E breaks down on oxidation. A typical example is shown in Fig. 6. Initial irradiation excites the (Re → bpy) MLCT state from which the (E → diimine) LLCT state is populated by an intramolecular $E \rightarrow Re^{II}$ electron transfer, oxidising the axial ligand that bears a 1,2-diamine-1,2-phenyl-ethyl group. However, the C–C bond of the oxidised 1,2-diamino group breaks down on a timescale competitive with the unproductive decay of the LLCT state to the ground state. Rate constants of 3×10^8 and 1×10^8 s^{-1} were determined for the C–C bond fragmentation k_{BF} and LLCT decay k_b, respectively [49]. A similar reactivity was observed for Re complexes with pyridine ligands bearing other 1,2-diamine or α-aminoalcohol groups [48,50,51]. Analogously, the $Re(N_3O_4CO)_3(bpy)^-$ complex, which contains the rather unusual dinitramide ligand $N_3O_4^-$ produces $Re(NO_3)(CO)_3(bpy)$, $Re(Cl)(CO)_3(bpy)$ and N_2O on irradiation in a CH_2Cl_2 solution [52]. Apparently, the ($N_3O_4^- \rightarrow$ bpy) LLCT state is populated from the initially excited MLCT state, resulting in a fragmentation of the dinitramide ligand. Generally, the observation of irreversible, oxidatively induced, reactions of the axial ligand upon initial (Re → bpy) MLCT excitation provides a clear evidence for the existence of a non-radiatively populated LLCT state. It also opens a possibility to investigate the mechanisms and dynamics of very fast reactions of oxidised axial ligands [49,50]. Synthetic or photocatalytic applications might follow.

3.4. Gradual change of the lowest excited state character from MLCT to LLCT for halide axial ligands

All the complexes containing a halide axial ligand exhibit a broad, structureless, rigidochromic emission band whose presence suggests a charge transfer character of the emissive excited state. Its decay is always dominated by the non-radiative mechanism, $k_{nr} \gg k_r$, rendering emission quantum yields well below 0.1. No systematic structural trends in the k_r values were found. An Arrhenius-type temperature dependence (Eq. (2)) of the non-radiative decay rate was observed in 2-Me–THF fluid solutions for the iodo species [77] Ru(I)(Me)$(CO)_2$(*i*Pr-DAB); $k_0 = 1.8 \times 10^6$ s^{-1}, $A = 7.4 \times 10^7$ s^{-1}, $E_a = 610$ cm^{-1}; Ru(I)(Me)$(CO)_2$(*i*Pr-PyCa); $k_0 = 4.8 \times 10^5$ s^{-1}, $A = 2.4 \times 10^8$ s^{-1}, $E_a = 960$ cm^{-1}; and for [72] Ru(Cl)$(SnPh_3)(CO)_2$(*i*Pr-DAB); $k_0 = 2.4 \times 10^5$ s^{-1}, $A = 1.1 \times 10^8$ s^{-1}, $E_a = 1009$ cm^{-1}. The values of the activation parameters, together with the photostability, indicate that the thermally activated decay pathway proceeds through another close-lying CT state, similar to the decay of the ^{3}MLCT excited states of Re(Cl)$(CO)_3$(bpy) or Re(4-Et-py)$(CO)_3(bpy)^+$ discussed earlier.

Surprisingly, inspection of Figs. 2 and 3 shows that the excited state lifetimes of Re(X)$(CO)_3$(α-diimine) or Ru(X)(R)$(CO)_2$(α-diimine) complexes increase sharply on changing the axial ligand X from Cl to Br and namely, to I while the emission energy hardly changes. The same behaviour occurs regardless of the diimine ligands used and, in the case of the Ru species, regardless of the *trans* alkyl ligand, R = Me or Et. Obviously, the effect of the halide on the rate of the non-radiative decay does not obey the EGL. This observation points to a change in the character of the emitting excited state as a function of the halide. This is further supported by the excited state absorption spectra (Fig. 7) of Re(X)$(CO)_3$(bpy) or Ru(X)(Me)$(CO)_2$(*i*Pr-DAB) that show an intense, nearly halide-independent, feature attributed to the reduced diimine$^{\bullet -}$ chromophore (DAB: 420 nm [78], bpy′: 375 and 470 nm [112]). In addition, another absorption feature, whose position and relative intensity are strongly halide-dependent, is apparent in the excited state spectra, see Fig. 7. For the chlorides, it occurs as a very weak red tail of the diimine$^{\bullet -}$ band. In the case of the bromides, it becomes a distinct low-energy shoulder while a separate, relatively intense, band develops at longer wavelengths for the iodides [e.g. at 780 and 590 nm for Re(I)$(CO)_3$(bpy) and Ru(I)(Me)$(CO)_2$(*i*Pr-DAB), respectively]. The presence of the spectral features due to the diimine radical-anions shows that, regardless the halide ligand used, the lowest excited state involves a CT to the diimine. This conclusion is corroborated by time-resolved Raman spectra of the lowest excited states of Ru(X)(Me)$(CO)_2$(*i*Pr-DAB), which show [78] a drop in the ν_s(CN) stretching frequency of the DAB ligand by 83, 71 and 65 cm^{-1} on the excitation for X = Cl, Br or I, respectively. However, the halide-dependent, low-energy band found in the excited state absorption spectra cannot be assigned to the diimine$^{\bullet -}$ chromophore. Its position and intensity indicates that the characters and energy spacings of the low lying excited states change as a function of the halide ligand.

Important information about the influence of the halide ligand on the excited state character of Ru(X)(Me)$(CO)_2$(*i*Pr-DAB) came from the time-resolved IR spectra [78]. Both ν(CO) IR bands were found to shift on excitation to higher frequencies, the magnitude of this shift decreasing in the order Cl(50, 51 cm^{-1}) > Br(48, 45 cm^{-1}) ≫ I(27, 43 cm^{-1}). [The values in parentheses show the differences in the ν(CO) wavenumbers between the excited and ground state for the high- and low-frequency ν(CO) bands, respectively.] Differences between the excited and

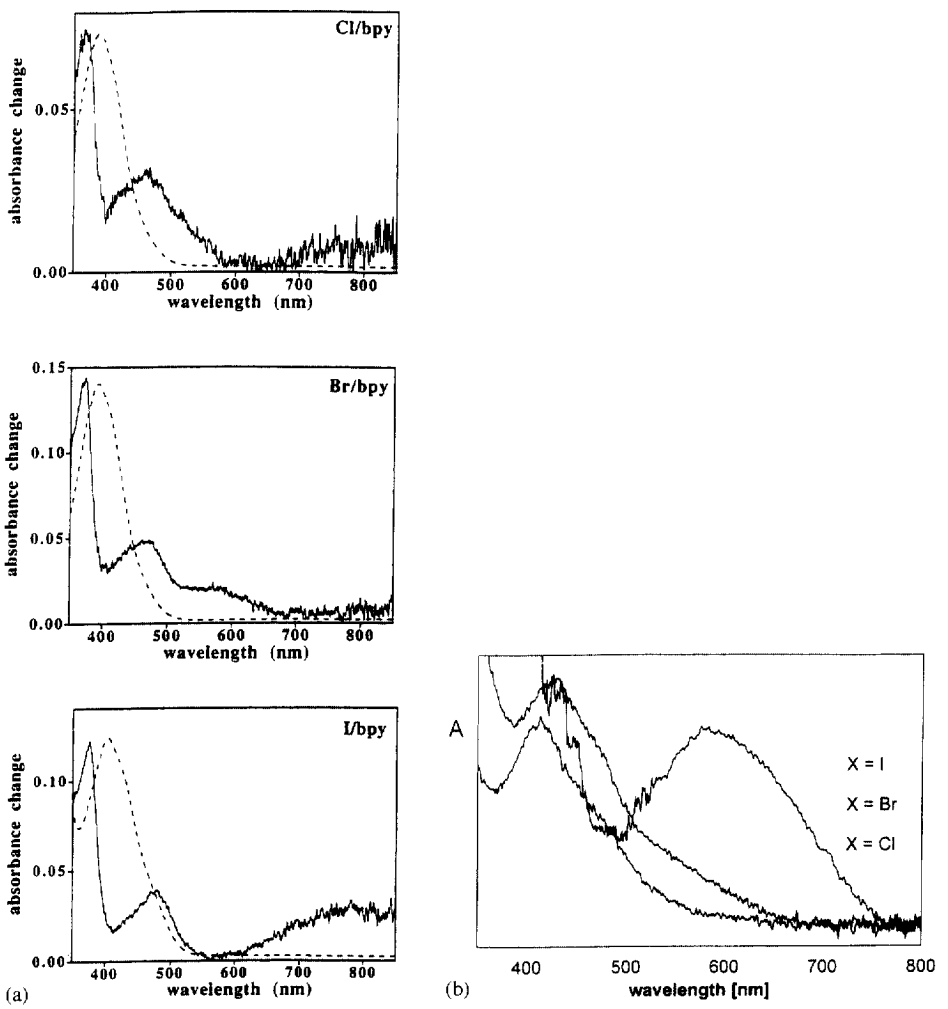

Fig. 7. (a) Visible absorption spectra of the excited (——) and ground (- - -) states of Re(X)$(CO)_3$(bpy); X = Cl, Br, I; complexes measured in THF [112]. The excited state spectrum was obtained 10 ns after laser excitation; (b) visible absorption spectra of the excited state of Ru(X)(Me)$(CO)_2$(*i*Pr-DAB); X = Cl, Br, I; complexes measured in THF 20 ns after laser excitation [78].

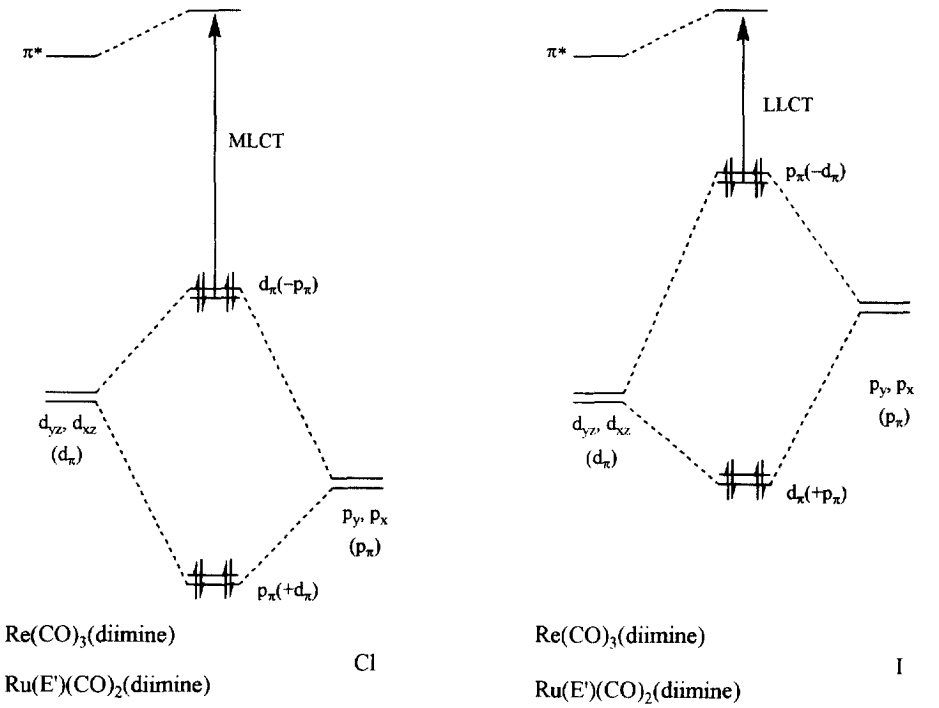

Fig. 8. Simplified MO scheme showing the effect of the π-interaction between the metal atom and the halide axial ligand on the character of the lowest electronic transition. Left: the two highest occupied molecular orbitals of the chloro complexes are predominantly of a metal d_π character, giving rise to an essentially (M → diimine) MLCT lowest transition. Right: the two highest occupied molecular orbitals of the iodo complexes are predominantly of an iodo p_π character, giving rise to a mostly (I → diimine) LLCT lowest transition.

ground state values of the CO stretching force constants decrease in the same order: Cl (82 N m^{-1}) > Br (76 N m^{-1}) ≫ I (55 N m^{-1}). The value found for the chloro complex is about the same as the average value measured [115] for the MLCT excited state of Re(Cl)(CO)$_3$(4,4'-bipyridyl)$_2$, 83 Nm^{-1}. The (Ru → DAB) MLCT character of the lowest excited state of Ru(Cl)(Me)(CO)$_2$(*i*Pr-DAB) and of other Ru(Cl)(R)(CO)$_2$(α-diimine) and Re(Cl)(CO)$_3$(α-diimine) complexes is, thus, well-established. The TRIR spectra show, however, that the extent of the 'oxidation' of the metal atom in the excited state decreases in the order Cl > Br ≫ I. This trend is readily understood by considering that the metal d_π orbitals and halide p_π orbitals overlap. Their interaction gives rise to M–X π-antibonding ($d_\pi - p_\pi$) and π-bonding orbitals ($d_\pi + p_\pi$), see Fig. 8. Because both the bonding and antibonding orbitals are occupied, the M–X π-interaction is repulsive. The M–X π-antibonding orbital becomes the HOMO of the complex molecule. Going down the halide group, the energy of the p_π orbital increases as the electron negativity of the halogen atom decreases. Hence, the halide participation in the HOMO increases in the order Cl < Br ≪ I. In the most simple way, the lowest electronic excitation may

be viewed as a HOMO → π^*-(diimine) transition. The mixed metal/halide character of the HOMO implies that the positive hole in the excited state is actually delocalised between the halide and the metal, i.e. that the lowest excited state has a mixed (M → diimine) MLCT and (X → diimine) LLCT character. Increasing halide participation in the HOMO causes the hole to be increasingly halide-localised. Hence, the character of the lowest excited state changes gradually from (M → diimine) MLCT to (X → diimine) LLCT while the halide ligand changes from Cl to Br and especially, to I.

The EGL map of the Ru(X)(E′)$(CO)_2$(α-diimine) complexes (Fig. 3) shows that the MLCT/LLCT character of the emitting excited state is also dependent on the second axial co-ligand E′ that is not involved in the (E → diimine) LLCT excitation. Thus, the decay of the excited state of Ru(Cl)$(SnPh_3)(CO)_2$(*i*Pr-DAB) is much slower than that of all its Ru(X)(Me)$(CO)_2$(*i*Pr-DAB) counterparts, despite essentially the same emission energy. TRIR spectra showed [72] that the ν(CO) frequencies of Ru(Cl)$(SnPh_3)(CO)_2$(*i*Pr-DAB) decrease by only 17 and 30 cm^{-1}, which amounts to a decrease of the CO stretching force constant by 38 Nm^{-1}, even less than for Ru(I)(Me)$(CO)_2$(*i*Pr-DAB). This indicates a (Cl → DAB) LLCT excited state. The same LLCT excited state probably occurs for E′ = $PbPh_3$ [72]. Fig. 3 also shows that the emission energy of the bromo and iodo alkyl complexes Ru(X)(R)$(CO)_2$(*i*Pr-DAB) (X = Br or I) decreases on replacing R = Me for Et. At the same time, the decay rate slightly decreases, contrary to the EGL. This trend indicates either increasing LLCT character of the emitting state for the ethyl complexes or a mixing with excited states derived from the axial σ-bonding orbitals, see Section 3.3.

The above qualitative interpretation of the halide and co-ligand effects on the mixed MLCT/LLCT nature of the lowest excited state were fully supported by the DFT-MO calculations of Ru(Cl)(Me)$(CO)_2$(H-DAB) and Ru(I)(Me)$(CO)_2$(H-DAB) model molecules, respectively [128]. Separate calculations were performed on the ground and excited states, allowing thus for the electronic relaxation. Apart from the state energies and oscillator strengths for individual transitions, changes in the population of individual atomic or fragment orbitals were also calculated. The lowest excited state was indeed found to involve charge transfer directed into the π^* diimine orbital whose population was calculated to increase by 0.42 and 0.53 electrons for the chloro and iodo complex, respectively. However, as expected, a different origin of the excited electron was calculated for the two complexes. For Ru(Cl)(Me)$(CO)_2$(H-DAB), the Ru-4d_{yz} and Cl-3p_y orbitals are depopulated on the lowest energy excitation by 0.32 and 0.21 electrons, respectively. The situation is reversed for the iodo complex for which the same orbitals are depopulated by 0.24 and 0.48 electrons, respectively, in line with a change of the excited state character from essentially MLCT to LLCT on going from Cl to I. Moreover, the calculations revealed an unexpected partial compensation of the decreased p_π electron density on the I ligand in the LLCT excited state by an increase in the population of the I-5p_z orbital, which is involved in the Ru–I σ-bonding. For Ru(Cl)$(SnPh_3)(CO)_2$(*i*Pr-DAB), depopulation of the Ru-4d_{yz} and Cl-3p_y orbitals on the excitation was calculated as 0.17 and 0.30 electron, respectively [72], supporting

the proposed predominant (Cl → DAB) LLCT character of the lowest excited state. The halide dependent d_π/p_π mixing in the HOMO also follows from calculations performed on Mn(X)(CO)$_3$(bpy) [129].

Having established that the character of the lowest excited state of the halide complexes Ru(X)(R)(CO)$_2$(α-diimine) and Re(X)(CO)$_3$(α-diimine) changes from (M → diimine) MLCT for X = Cl to mostly (X → diimine) LLCT in the case of X = I, it remains to discuss why the rate of the non-radiative excited state decay decreases with increasing LLCT character. The first clue is provided by the values of the apparent Stokes shift $\Delta E_{\text{asb-em}}$, which drop by 1100–1800 cm^{-1} (depending on the metal, diimine and/or R) on going from Cl to I. This trend indicates that the excited state distortion and the decay rate decrease in parallel, Cl > Br > I. ($\Delta E_{\text{abs-em}}$ is defined as the difference between the absorption and emission maxima. Hence, it includes the distortion-related term $\hbar\omega_m\Delta_m^2$ plus the singlet–triplet splitting, which is assumed to be largely ligand-independent.) The much smaller effect of the LLCT than MLCT excitation on the CO ligands appears to contribute to the smaller molecular distortion in the LLCT state. Consequently, the role of the ν_s(CO) vibration as an intramolecular acceptor mode and its coupling to the solvent librations are diminished and values of both ω_m and χ_0 will decrease, affecting k_0 accordingly (Eq. (4)). The intra-diimine bonds are also slightly less distorted in the LLCT than MLCT states, as was shown by the time-resolved rR spectra of Ru(X)(Me)(CO)$_2$(*i*Pr-DAB), vide supra. Effects of the LLCT excitation on the M–I bond appears to be rather small, as was documented by a low intensity of the ν(M–I) peak found in the rR spectra of some of the iodo complexes [76,112,130]. Weakening of the electronic coupling to the ground state (β in Eq. (4)) on changing the excited state character from MLCT to LLCT is probably another important factor responsible for slowing down the non-radiative decay.

The (X → diimine) LLCT excited states are mostly stable toward photochemical ligand dissociation. The only exception seems to be Ru(I)(Me)(CO)$_2$(bpy′) which undergoes a photochemical *trans* → *cis* isomerisation that involves a CO loss [123]. However, no bonds in other Ru(I)(R)(CO)$_2$(α-diimine), Re(I)(CO)$_3$(α-diimine) (R = Me or Et) or Ru(Cl)(SnPh$_3$)(CO)$_2$(α-diimine) (diimine = PyCa, DAB) complexes are weakened significantly by LLCT excitation. The long LLCT excited state lifetimes are favourable for bimolecular excited state reactions. Indeed, electron- and energy-transfer quenching of the LLCT state was observed for Ru(I)(R)(CO)$_2$(α-diimine) (R = Me or Et) [77].

In Section 3.2, it was shown that the (L → diimine) LLCT transitions in complexes with oxidisable ligands are extremely weak due to very small electronic overlap of the orbitals involved. However, the situation is profoundly different for the complexes Ru(X)(R)(CO)$_2$(α-diimine) and Re(X)(CO)$_3$(α-diimine) (X = Cl, Br, or I; R = Me or Et). The halide p_y and the π^*-(diimine) orbitals are directly coupled by sharing an overlap with the metal d_{yz} orbital. Moreover, a through-space p_y–π^* interaction is also possible. Hence, the (X → diimine) LLCT transitions are expected to occur with an intensity comparable or slightly lower than that of MLCT transitions. Indeed, all the Ru(X)(R)(CO)$_2$(α-diimine) and Re(X)(CO)$_3$(α-diimine) (X = Cl, Br, or I; R = Me or Et) complexes exhibit [76,112] an intense (ϵ in the range

2200–1500 M^{-1} s^{-1} for Ru and 4100–2100 M^{-1} s^{-1} for Re), solvatochromic, absorption band in the visible spectral region, see Fig. 9. The maximum of the lowest absorption band shifts only slightly to longer wavelengths on going down the halide series. The integrated intensity of the lowest band of $Re(X)(CO)_3(\alpha$-diimine) is comparable for X = Cl and Br, but it halves on going to I [112]. For the Ru species, only a small gradual decrease in molar absorptivity on going from Cl to Br and I was observed [76]. The broad, unresolved, band shape is almost identical for the Cl and Br complexes whereas a poorly resolved vibrational structure of ca. 1200 cm^{-1} appears for some of the iodo complexes. This may be caused by a weaker coupling with solvent librations (smaller χ_0) due to smaller charge change on the CO ligands in the LLCT state. Raman spectra of several iodo Ru or Re complexes measured in (pre)resonance with the lowest electronic transition show [77,112] a

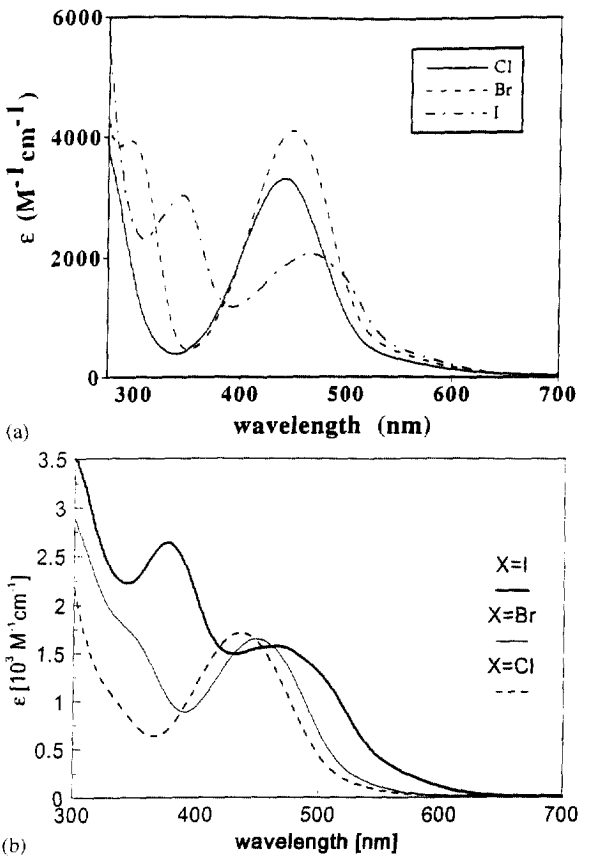

Fig. 9. (a) Electronic absorption spectra of $Re(X)(CO)_3(i$Pr-DAB); X = Cl, Br, I; measured in THF at r.t. [112]; (b) electronic absorption spectra of $Ru(X)(Me)(CO)_2(i$Pr-DAB); X = Cl, Br, I; measured in THF at r.t. [76].

pattern of enhanced peaks which is fully in line with the excited state distortions discussed above. The most enhanced peak belongs to the ν_s(CN) intra-diimine vibration, in accordance with the LLCT transition being directed to the diimine ligand. The ν_s(CO) Raman peak is either very weak or missing completely since the LLCT transition does not originate in the $Re(CO)_3$ or $Ru(CO)_2$ moiety. A weak peak due to the ν(Ru–Br) vibrations was identified [130] in the rR spectrum of $Re(Br)(CO)_3$(pTol-DAB) at 190 cm^{-1}. Similar weak peaks that could be attributed to Re–X or Ru–X vibrations occur in the rR spectra of other bromo and iodo complexes [77,112].

3.5. Introduction of $\sigma\pi^*$ state by covalently bound axial ligands

One of the most fascinating aspects of the photochemistry of Re and Ru carbonyl diimine complexes is to follow how small changes in their coordination spheres completely alter their photochemical reactivity. For example, the $Ru(R)(I)(CO)_2$(*i*Pr-DAB) complexes are photochemically stable [77] for R = Me and Et, whereas their isopropyl analogue [56] $Ru(iPr)(I)(CO)_2$(*i*Pr-DAB) is highly photoreactive. It undergoes an efficient homolysis of the Ru–C(*i*Pr) bond on irradiation into its lowest absorption band. In fact, efficient metal–ligand bond homolysis producing radicals is a characteristic photochemical reaction of those Re and Ru carbonyl diimine complexes which contain alkyl, benzyl, or metal-coordinated axial ligands [3,46,53,54,56–61,63–67,69–75,84,109,131]. With a few noteworthy exceptions, the metal–ligand homolysis occurs with a high quantum yield ($\phi > 0.1$) which is independent of the temperature and excitation wavelength λ_{exc}. This is the case of the reactions:

$$Re(E)(CO)_3(\alpha - \text{diimine}) \overset{h\nu, S}{\rightarrow} E^{\cdot} + Re(S)(CO)_3(\alpha - \text{diimine})^{\cdot}, \quad (8)$$

where E = Et, *i*Pr, benzyl (Bz), $Re(CO)_5$, $Mn(CO)_5$, $Co(CO)_4$; diimine = phen, bpy, R-Pyca, R-DAB; and

$$Ru(E)(E')(CO)_2(\alpha - \text{diimine}) \overset{h\nu, S}{\rightarrow} E^{\cdot} + Ru(S)(E')(CO)_2(\alpha - \text{diimine})^{\cdot}, \quad (9)$$

where E = *i*Pr, $SnPh_3$, $GePh_3$, $Mn(CO)_5$, $Re(CO)_5$, $CO(CO)_4$; E′ = alkyl or another metal fragment, but not a halide.

$Re(Me)(CO)_3$(α-diimine) [53,54,57,60,61] and $Ru(SnPh_3)_2(CO)_2$(*i*Pr-DAB) [72] complexes undergo qualitatively similar photoreactions. However, their quantum yields are lower and strongly dependent on the temperature and, in the former case, on the excitation wavelength. Although the photochemistry of these species involves the same type of excited state as their more reactive counterparts, the detailed mechanisms are somewhat different and will be discussed separately.

Formation of radicals in Eqs. (8) and (9) has been amply demonstrated by their direct observation with EPR [66] or FT-EPR [59] or by the formation of characteristic products of secondary radical reactions. EPR data show that the solvated radicals $Re(S)(CO)_3\alpha$-diimine)$^{\cdot}$ and $Ru(S)(E')(CO)_2$(α-diimine)$^{\cdot}$ are formally complexes of Re^{I} and Ru^{II}, respectively, with radical-anions of the diimines. Alkyl radicals were detected [59,60] directly by FT-EPR already at 10 ns after excitation

of $Re(R)(CO)_3(bpy')$ (R = Me, Et, *i*Pr or Bz) or $Ru(R)(I)(CO)_2(i$Pr-DAB) (R = *i*Pr or Bz). Detection of the radical products in inert solvents (hydrocarbons, THF) and the kinetics of their formation (studied by time-resolved visible or IR absorption spectra and by FT-EPR) indicate that the homolytic splitting of the axial metal–ligand bond is the primary photochemical step which occurs directly from a reactive excited state that is populated via the optically excited ^{1}MLCT state.

The photoproduced radicals often undergo interesting secondary reactions. Photolysis in the presence of radical scavengers like CCl_4, $CHCl_3$ or CH_2Cl_2 produces chloro complexes $Re(Cl)(CO)_3(\alpha$-diimine) or $Ru(Cl)(E')(CO)_2(\alpha$-diimine), together with ECl adducts or E–E dimers, depending on E and the solvent. Formation of radical adducts of E$^{\cdot}$ was observed by EPR on irradiation of THF or hydrocarbon solutions in the presence of spin traps nitrosodurene or *t*BuNO. Radicals $Re(S)(CO)_3(\alpha$-diimine)$^{\cdot}$ and $Ru(S)(E')(CO)_2(\alpha$-diimine)$^{\cdot}$ become highly reducing when the solvent (S) is strongly bound. Thus, light-induced electron transfer chain reactions were observed in coordinating solvents and/or in the presence of ligands like PPh_3 [56,65,68,71]. Photochemical isomerisation of $Re[Mn(CO)_5](CO)_3(i$Pr-DAB) [64] or $Ru[Mn(CO)_5](Me)(CO)_2(i$Pr-PyCa) [71] to dinuclear complexes with bridging DAB or PyCa ligands, respectively, was observed in apolar inert solvents. Dimerisation to the metal–metal bonded dimers $Re_2(CO)_6(\alpha$-diimine$)_2$ or $RU_2(E')_2(CO)_4(\alpha$-diimine$)_2$ is another common reaction of photoproduced organometallic radicals [71,75].

The appearance of a photochemical reaction on changing the axial ligands in Re and Ru carbonyl–diimine complexes from halides or other Lewis bases (pyridines, phosphines, etc.) to alkyls or metal fragments [e.g. $SnPh_3$, $Mn(CO)_5$ or $Re(CO)_5$] implies a profound change in the character of the lowest excited state. This is well-demonstrated by the EGL maps shown in Figs. 2 and 3. It is evident that the emission from the photoreactive metal–metal or metal–alkyl bonded complexes comprises a distinct region in the EGL maps that is far apart from that of the MLCT or LLCT emission from the halides. Both the emission energy and the non-radiative decay rate decrease significantly on going from the halide complexes to those containing a metal–metal or a metal–alkyl bond, in an obvious violation of EGL. This observation can be accounted for by a completely different character of the emissive excited state and mechanism of its non-radiative decay. On the other hand, the rather good EGL correlation found within the families of the metal-containing or alkyl complexes indicates a common nature of their lowest excited states. Besides the unusually long lifetimes and low energies, the dinuclear or alkyl complexes show some features suggesting a CT character of the emissive excited state. The emission bands are broad and structureless. However, apparent Stokes shift values, $\Delta E_{abs\text{-}em}$, are smaller than those of the halide complexes by some 2000 cm^{-1}. No clear correlation between τ and $\Delta E_{abs\text{-}em}$ was found, although species containing the $SnPh_3$ ligand have the longest lived excited states and the smallest Stokes shifts. Compared with analogous complexes that emit from MLCT or LLCT states, the radiative rate constants measured for the dinuclear or alkyl complexes are 10–100 times smaller. All the dinuclear complexes studied are emissive in a low-temperature (80 K) 2-Me–THF glass while the only emissive alkyl complexes

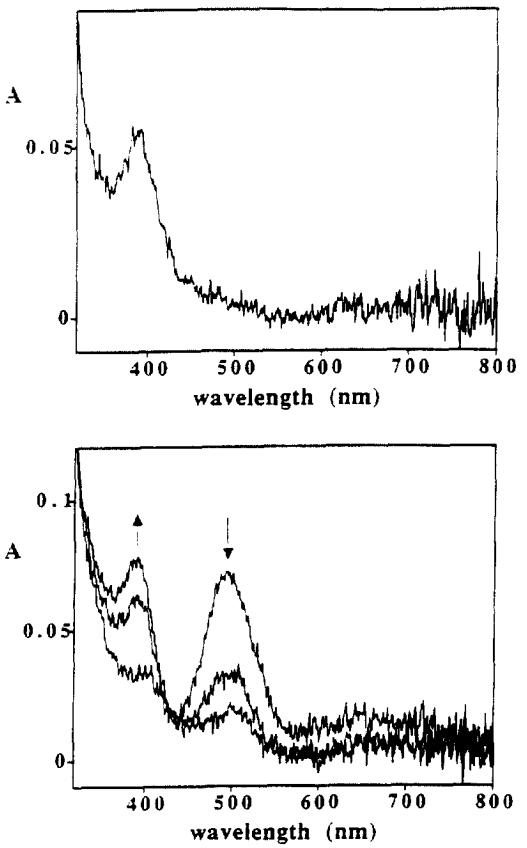

Fig. 10. Time-resolved visible absorption spectra of $Re(Bz)(CO)_3(iPr\text{-}DAB)$ measured at 30 ns after excitation [57]. Top: spectrum obtained in 2-Me–THF. Only those features are observed that belong to the photoproduced solvated $Re(CO)_3(iPr\text{-}DAB)^{\cdot}$ radicals. Bottom: spectrum obtained in toluene. The band due to the $\sigma\pi^*$ excited state at ca. 500 nm gradually decreases while the band at ca. 390 nm due to solvated $Re(CO)_3(iPr\text{-}DAB)^{\cdot}$ radicals increases with the same lifetime, 250 ns.

are $Re(Me)(CO)_3(bpy')$ [53,60], unreactive $Re(Ph)(CO)_3(bpy')$ [53,60] and $Ru(E)(Me)(CO)_2(iPr\text{-}DAB)$ [72] in which E = metal fragment. Rigidochromism was observed [62,72] for those few compounds that are emissive in fluid solutions, i.e. $Re(Me)(CO)_3(bpy')$, $Re(SnPh_3)(CO)_3(\alpha\text{-diimine})$ (diimine = bpy, phen) and $Ru(SnPh_3)_2(CO)_2(iPr\text{-}DAB)$.

Studies on $Re(Bz)(CO)_3(iPr\text{-}DAB)$ were most revealing [57,58] with respect to the characterisation of the reactive excited state. Irradiation into the lowest absorption band of this complex produces benzyl and solvated $Re(CO)_3(iPr\text{-}DAB)^{\cdot}$ radicals with a quantum yield of ca. 0.8 which is independent of temperature (273–253 K) and λ_{exc} (varied within the lowest absorption band), as well as of the solvent (toluene or THF). Nanosecond time-resolved IR and UV–vis spectra (Figs. 10 and 11) measured from THF solutions or other polar and/or coordinating solvents

(2-Me–THF, CH_3CN, 2-Cl-butane) show only features due to the $Re(S)(CO)_3$(*i*Pr-DAB)$^{\cdot}$ radical, with no hint of a signal due to the excited state. Picosecond spectra reveal that the bond homolysis in the THF solution is fully completed within 30 ps. However, the situation changes dramatically in non-polar non-coordinating solvents: toluene, benzene or cyclohexane. Both the time-resolved IR and UV–vis spectra show transient features due to an excited state that converts into the radicals with a rate constant of 4×10^6 s^{-1} ($\tau = 250$ ns) with no appreciable parallel decay to the ground state. The UV–vis spectrum (Fig. 10) of this excited state shows an intense peak at 500 nm. In addition, the weak, broad, transient absorption at around 650 nm and the strong absorption in the UV indicate the presence of an *i*Pr-DAB$^{\cdot -}$ chromophore. The TR-IR spectrum (Fig. 11) shows features at 2015 and ca. 1910 cm^{-1} which are very close to the IR bands of the ground state (2007, 1918, 1909 cm^{-1}). The shift of the excited state ν(CO) frequencies from their ground-state values is surprisingly small, much smaller than that observed for LLCT or MLCT excited states, vide supra. This observation indicates that the excitation causes only a very small, if any, decrease of the electron density at the $Re(CO)_3$ moiety. In other words, the excited electron does not originate in any

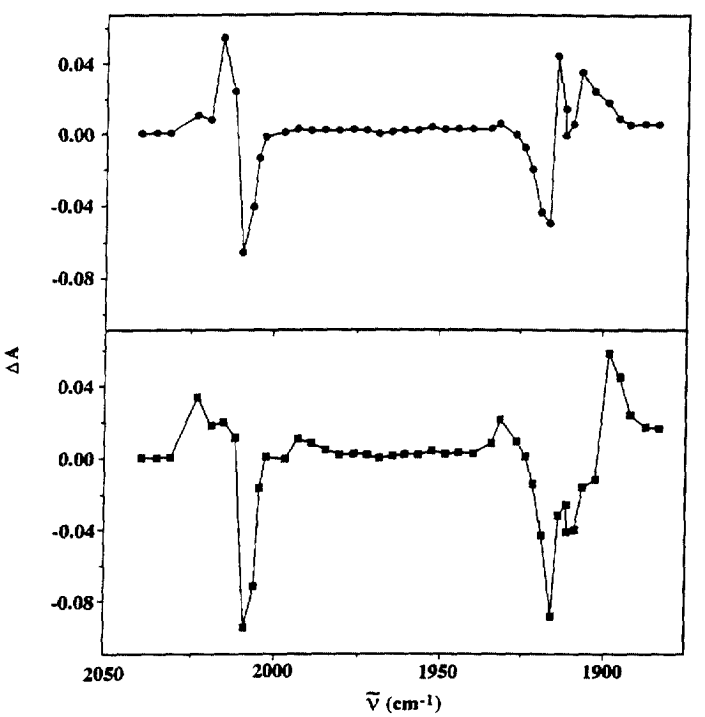

Fig. 11. Time-resolved IR spectra of $Re(Bz)(CO)_3$(*i*Pr-DAB) measured in *n*-heptane [57]. Negative bands correspond to bleached ground state while the positive ones belong to the photoproduced transients. Top: spectrum obtained at 100 ns after excitation corresponds to the $\sigma\pi^*$ state. Bottom: spectrum obtained at 3.5 μs corresponds to the solvated $Re(CO)_3$(*i*Pr-DAB)$^{\cdot}$ radical.

molecular orbital to which the Re d_π orbitals contribute. This observation, the UV–vis indication that the excited electron is localised on the DAB ligand, and the labilisation of the Re–Bz bond on excitation point to a $\sigma\pi^*$ character of the lowest excited state. Such an excited state involves excitation of an electron from the Re–C(Bz) σ-bonding orbital to the π^* orbital of the DAB ligand. The excited state may be viewed as a $Bz^{\cdot}$-$Re^{I}(CO)_3(i\text{Pr-DAB}^{\cdot -})$ species in which the benzyl ligand is bound to the metal atom by a one-electron σ bond. The decrease of the electron density at the metal centre on the $\sigma\pi^*$ excitation is very small because the depopulated σ-bonding orbital has mostly a benzyl character. In addition, the CIDEP and spin-polarisation effects observed in the FT-EPR spectra obtained for $Re(R)(CO)_3(bpy')$ (R = Me, Et, *i*Pr or Bz) and $Ru(R)(I)(CO)_2(i\text{Pr-DAB})$ (R = *i*Pr or Bz) determined the spin state of the reactive $\sigma\pi^*$ state as a triplet [59,60]. A $^3\sigma\pi^*$ excited state has been proposed earlier, albeit without a spectroscopic evidence, to account for the Re–Sn photochemical bond homolysis of $Re(SnPh_3)(CO)_3(phen)$ [3,62,63].

The photochemical behaviour of $Re(Bz)(CO)_3(i\text{Pr-DAB})$ is paradigmatic for the whole class of Re and Ru dinuclear and alkyl complexes. Salient aspects of their photochemistry are summarised in Table 1. In many cases, the $^3\sigma\pi^*$ state was detected directly by the observation of an intense transient absorption feature that occurs in the visible spectral region. Overlap with the bleach usually prevents the accurate determination of the lifetime. Hence, only the upper-limits, listed in Table 1, were estimated. In most cases, the chemical reaction is the main decay pathway of the $^3\sigma\pi^*$ state at r.t. since the non-radiative transition to the ground state is very slow. The dramatic acceleration of the Re–E bond homolysis in coordinating and/or polar solvents from the nanosecond to sub-picosecond time domain was observed [57,58,73] for $Re(E)(CO)_3(i\text{Pr-DAB})$ E = Bz, Et, $Mn(CO)_5$ or $Re(CO)_5$. Even the $^3\sigma\pi^*$ lifetimes of the relatively unreactive $Re(SnPh_3)(CO)_3(\alpha\text{-diimine})$ complexes decrease about twice on going from toluene to THF [73]. The photochemical quantum yield increases profoundly in chlorinated solvents. Coordinating and/or polar solvents facilitate the bond homolysis either by an attack on the weakened one-electron metal–ligand bond present in the $^3\sigma\pi^*$ excited state and/or by changing the energetics of the reaction, vide infra. On the other hand, $Re(R)(CO)_3(bpy')$ (R = Et, *i*Pr, or Bz) and most of the Ru complexes react so fast that the $^3\sigma\pi^*$ state was not observed on a nanosecond time scale even in hydrocarbon solvents. FT-EPR spectra revealed [59] that the M–C(R) bond homolysis in $Re(R)(CO)_3(bpy')$ (R = Et, *i*Pr, or Bz) and $Ru(R)(I)(CO)_2(i\text{Pr-DAB})$ (R = *i*Pr, Bz) is fully completed within 10 ns ($> 10^8\ s^{-1}$). A femtosecond rate of the Re–R bond homolysis was found for $Re(R)(CO)_3(bpy')$ complexes (R = Me, Et) [132]. Homolysis of Ru–$Mn(CO)_5$, Ru–$Re(CO)_5$ and Ru–Me [in $Ru(Me)(SnPh_3)(CO)_2(i\text{Pr-DAB})$] is also a sub-nanosecond (perhaps even a sub-picosecond) process [75].

The photophysical and photochemical studies discussed previously have firmly established the $^3\sigma\pi^*$ character of the lowest excited state of those $Re(E)(CO)_3(\alpha\text{-diimine})$ and $Ru(E)(E')(CO)_2(\alpha\text{-diimine})$ complexes in which E is an alkyl (Et, *i*Pr or Bz) or a metal fragment $Mn(CO)_5$, $Re(CO)_5$, $SnPh_3$, etc. and the second axial ligand E′ is not a halide (with the exception of the *i*Pr/X and Bz/X axial ligand

Table 1
Summary of the photochemical M–E homolytic dissociation reactivity in $Re(E)(CO)_3(\alpha\text{-diimine})$ and $Ru(E)(E')(CO)_2(\alpha\text{-diimine})$ complexes

Complexes that undergo relatively slow, solvent-dependent photochemical bond homolysis on ns–μs timescale. $^3\sigma\pi^*$ state detected spectroscopically in inert solvents		
$Re(SnPh_3)(CO)_3$(phen)	EPA	1.8 μs [63]
	CCl	1.8 μs; $\phi = 0.23$; $k_{homol} = 1.0 \times 10^5$ s^{-1} [63]
$Re(GePh_3)(CO)_3$(phen)	EPA	2.6 μs [63]
	CCl	2.5 μs; $\phi = 0.27$; $k_{homol} = 1.3 \times 10^5$ s^{-1} [63]
$Re(SnPh_3)(CO)_3$(bpy′)	Tol	1.1 μs [73]
	THF	500 ns; $\phi \cong 0.03$ in THF [73]
$Re(SnPh_3)(CO)_3$(*i*Pr-PyCa)	Tol	465 ns [73]
	THF	345 ns [73]
$Re(SnPh_3)(CO)_3$(*i*Pr-DAB)	Tol	140 ns; 60% decay to GS, 40% homolysis [73]
	THF	<100 ns[a]; 30% decay to GS, 70% homolysis [73]
	CCl	$\phi = 0.55$ [73]
$Re(Bz)(CO)_3$(*i*Pr-DAB)	Tol	250 ns; $\phi = 0.75$; $k_{homol} = 4 \times 10^6$ s^{-1} [57,58]
	Benz	90 ns [58]
	Chex	155 ns [58]
	THF	<30 ps[b] [58]
$Re(Bz)(CO)_3$(*t*Bu-DAB)	Tol	275 ns [58]
$Re(Et)(CO)_3$(*i*Pr-DAB)	Tol	60 ns [58]
$Re(Et)(CO)_3$(*t*Bu-DAB)	Tol	60 ns [58]
$Re(Et)(CO)_3$(*i*Pr-PyCa)	Tol	20 ns [58]
$Re(Mn(CO)_5)(CO)_3$(*i*Pr-DAB)	Tol	<100 ns[a] [73]
	THF	<10 ns[b] [73]
$Re(Mn(CO)_5)(CO)_3$(bpy′)	Tol	<400 ns[a] [73]
$Re(Re(CO)_5)(CO)_3$(bpy′)	Tol	<2.5 ns[a] [73]
	CHCl	<30 ps[b] [73]
$Re(Re(CO)_5)(CO)_3$(*i*Pr-bAB)	Tol	<275 ns[a] [73]
	THF	<10 ns[b] [73]
$Ru(SnPh_3)_2(CO)_2$(*i*Pr-DAB)	THF	1 μs; ϕ, τ are *T*-dependant [72,75]
	Hex	
$Ru(SnPh_3)(GePh_3)(CO)_2$-(*i*Pr-DAB)	THF	500 ns; homolysis: 60% Ru–Ge + 40% Ru–Sn [75]
	Hex	
$Ru(Mn(CO)_5)(Me)(CO)_2$-(*i*Pr-DAB)	Hex	<5 μs[a] (?); no GS recovery [71]
	THF	<10 ns[b] [71]
$Ru(Mn(CO)_5)(Me)(CO)_2$-(*i*Pr-PyCa)	Hex	Ru–Mn homolysis leads to isomerization [71]
Complexes which undergo very fast photochemical homolysis regardless of the solvent. $\sigma\pi^*$ state not observed spectroscopically		
$Re(Et)(CO)_3$(bpy)	<10 ns[b] in toluene, 2-propanol [59]	
$Re(iPr)(CO)_3$(bpy′)	<10 ns[b] in toluene, 2-propanol [59]	
$Re(Bz)(CO)_3$(bpy′)	<10 ns[b] in toluene, 2-propanol [59]	

Table 1 (*Continued*)

Ru(*i*Pr)(I)$(CO)_2$(*i*Pr-DAB)	< 10 ns[b] in toluene, 2-propanol [59] Very weak $^3\sigma\pi^*$ absorption ($\tau < 10$ ns[a]) indicated in hexane, absent in THF [56]
Ru(Bz)(I)$(CO)_2$(*i*Pr-DAB)	< 10 ns[b] in toluene, THF [59]
Ru(Bz)(I)$(CO)_2$(bpy′)	< 10 ns[b] in toluene, THF
Ru($SnPh_3$)(Me)$(CO)_2$-(*i*Pr-DAB)	< 10 ns[b] in hexane, THF; Ru–Me split [75]
Ru($SnPh_3$)($Mn(CO)_5$)$(CO)_2$-(*i*Pr-DAB)	< 10 ns[b] in hexane, THF; Ru–Mn split [75]
Ru($Mn(CO)_5)_2(CO)_2$(*i*Pr-DAB)	< 10 ns[b] in hexane, THF [75]
Ru($Re(CO)_5)_2(CO)_2$(*i*Pr-DAB)	< 10 ns[b] in hexane, THF [75]
Ru($Re(CO)_5$)(Me)$(CO)_2$-(*i*Pr-DAB)	Ru–Re split [75]
Complexes in which the $\sigma\pi^*$ state lies above MLCT. It was not detected spectroscopically. Photochemical quantum yield depends on λ_{exc} and T	
Re(Me)$(CO)_3$(bpy′) [60]	
Re(Me)$(CO)_3$(*i*Pr-PyCA) [54,57]	
Re(Me)$(CO)_3$)(*i*Pr-DAB) [54,57]	

[a] Upper limit of the $\sigma\pi^*$ lifetime. Transient $\sigma\pi^*$ absorption observed, but accurate τ value was not determined because of strong overlap with the bleached ground state absorption.

[b] Bond homolysis fully completed within specified time delay after excitation. Values given are limited by the instrumental time-resolution. Actual homolysis lifetimes may be much shorter. Solvent abbreviations: EPA, ethanol/isopentane/ether (2/5/5); Tol, toluene; CCl, 0.5 M CCl_4 in $CHCl=CH_2Cl_2$ or THF; Benz, benzene; Chex, cyclohexane; Hex, hexane.

combinations). The $\sigma\pi^*$ state is introduced into the energetic region below that of the MLCT or LLCT states by the alkyl or metal-coordinated axial ligands whose high-lying σ-orbital energetically nearly matches the d_{z^2} or p_z σ-orbitals of the Ru or Re central metal atoms. Such Re–E or Ru–E bonds are covalent rather than coordinative and, according to the UV-photoelectron spectra [133], the corresponding σ-bonding orbitals occur above the d_π ones. Hence, the $\sigma\pi^*$ excited state lies below the MLCT or LLCT states. This situation is schematically depicted in Fig. 12.

The properties and reactivity of the $\sigma\pi^*$ state itself are strongly dependent not only on the σ-bonding properties of the ligand E, but also on the overall distribution of the electron density and bonding situation along the axial E–Re–CO and E–Ru–E′ bonds, respectively, (z-axis, see Fig. 1). In the Re complexes, the CO σ-orbitals lie well below the σ-orbitals of the E-ligands. The axial E–Re–CO bond may essentially be viewed as composed of two localised σ-bonds, Re–C and Re–E, respectively. The $\sigma\pi^*$ excited state involves only the Re–E σ-bonding orbital. Interestingly, for many of the Re complexes studied, the depopulation of the σ orbital in the excited state does not lead to a spontaneous bond splitting on a dissociative potential energy surface, unless assisted by an interaction with a polar solvent [57,58,73]. Instead, the $^3\sigma\pi^*$ state is a bound state with a well-defined

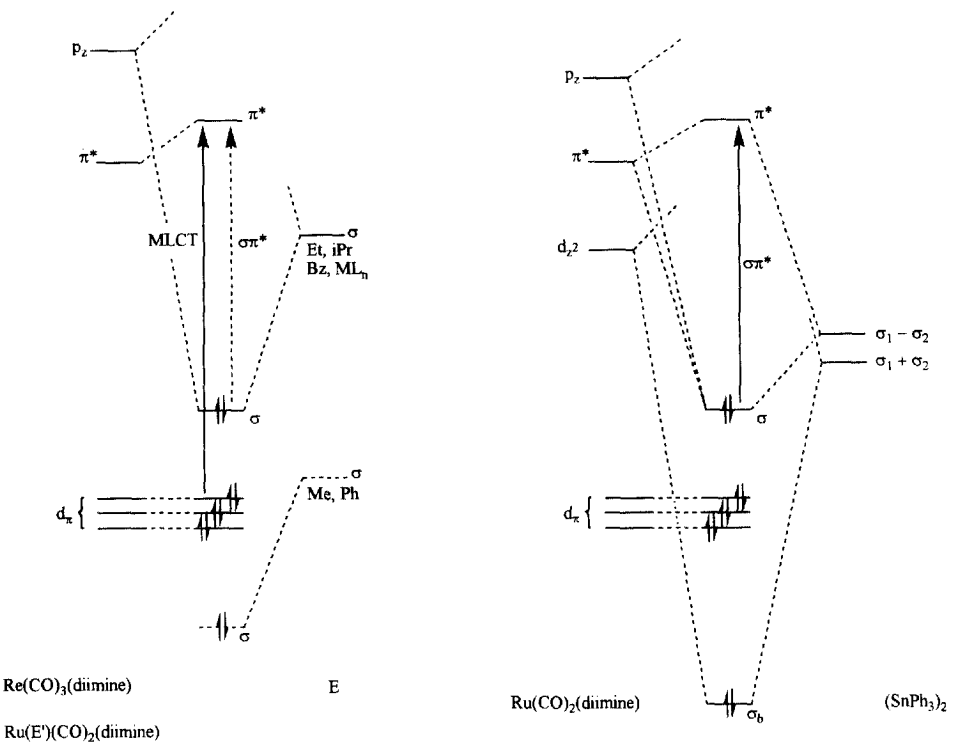

Fig. 12. Simplified MO diagram showing how $\sigma\pi^*$ becomes the lowest excited state in complexes with covalently bound axial ligands. Left: Re(E)$(CO)_3$(α-diimine) complexes. The occupied Re–E σ-bonding orbital lies above the d_π orbitals for axial ligands like Et, *i*Pr, Bz, metal fragments. Hence, the $\sigma\pi^*$ excited state lies below the MLCT one. On the other hand, axial ligands like Me or Ph are bound more strongly to the metal by lower-lying σ-orbitals. The resulting $\sigma\pi^*$ excited state, thus, lies above the MLCT one, although the energy difference is rather small, especially for Me. The σ-bonding orbital corresponding to the Re–CO axial bond lies always much lower in energy and, hence, the two axial bonds, Re–E and Re–CO, respectively, are essentially localised. A similar MO scheme would apply to Ru(E)(E')$(CO)_2$(α-diimine) complexes with chemically very dissimilar axial ligands; E ≠ E' ≠ halide. Right: $Ru(SnPh_3)_3(CO)_2$(*i*Pr-DAB) and Ru(E)(E')$(CO)_2$(α-diimine) complexes with chemically very similar axial ligands. The HOMO is predominantly composed of an antisymmetric combination of the σ orbitals of the two axial ligands with an admixture of the Ru $5p_z$ orbital. Note the strong interaction with the π^*(DAB) orbital which is responsible for the $\sigma-\pi^*$ delocalisation (see text) and makes the $\sigma \rightarrow \pi^*$ electronic transition strongly allowed.

energetic minimum. The one-electron E'–Re bond is still strong enough to dissociate only on a timescale of tens to hundreds of nanoseconds or, for Ph_3Sn, even longer. In general, the reactivity of the $^3\sigma\pi^*$ state in the Re complexes seems to be determined mostly by the strength of the Re–E bond, which influences the shape of the $^3\sigma\pi^*$ potential energy surface, namely the depth of its energetic minimum relative to the Re–E dissociation limit and/or to the activation barrier. Accordingly, the reactivity increases in the order $Ph_3Sn \ll Bz < Et < M(CO)_5$. Keeping the axial ligand constant, a decrease in reactivity with decreasing energy of the $^3\sigma\pi^*$

excited state is expected. Indeed, except for the Ph_3Sn complexes, the reactivity of the $^3\sigma\pi^*$ state decreases as a function of the diimine ligand in the order bpy′ > PyCa > DAB. The $^3\sigma\pi^*$ state is stabilised in this order by decreasing the energy of the π^*(diimine) orbital. These considerations also help to understand the solvent effect on the $^3\sigma\pi^*$ reactivity: an increase in the energy of the $^3\sigma\pi^*$ state relative to the energy of the radical products or to the activation barrier may also contribute to higher reaction rates in polar/coordinating solvents that would destabilise the $\sigma\pi^*$ state by solvatochromism and stabilise the radical products by solvation.

The situation becomes somewhat more complicated for the Ru(E)(E′)$(CO)_2$(α-diimine) complexes because of the synergism between the two axial ligands E and E′. Irradiation of complexes with highly dissimilar axial ligands leads to a rather fast (< 10 ns) homolysis of the weaker of the Ru–E and Ru–E′ bonds [75]. However, complexes in which the two E ligands are identical, like in $Ru(SnPh_3)_2(CO)_2$(*i*Pr-DAB) [72], show a rather different behaviour. The equivalence of the two axial bonds gives rise to a delocalised three centre, four electron, Sn–Ru–Sn bond [82]. The highest occupied axial σ molecular orbital, which is also the HOMO of the complex molecule, is composed of the antisymmetric combination of the two Sn lone electron pairs (49%) and the Ru-5p_z orbital (12%). Importantly, the π^*(DAB) orbital mixes with this axial σ orbital, contributing to the HOMO by 24%. This strong $\sigma-\pi^*$ interaction has profound consequences even on the ground state structural, electrochemical and spectroscopic properties [82]. It occurs even in the LUMO, which is composed of 66% π^* orbital, 9% d_{yz} orbital and 25% Sn σ-orbitals. [All orbital compositions were calculated [72,82] by DFT-MO for $Ru(SnH_3)_2(CO)_2$(H-DAB).] The HOMO → LUMO excitation, which gives rise to the $\sigma\pi^*$ excited state, has only very little structural effects. The Sn–Ru–Sn bond is virtually not labilised because of only weakly bonding character of the depopulated σ orbital. The net σ-depopulation is rather small anyway since the Sn σ-orbitals contribute to both the HOMO and LUMO. DFT-MO calculations estimated [72] that the Sn σ and Ru-5p_z orbitals are depopulated on the $\sigma\pi^*$ excitation by only 0.09 and 0.13 electrons, respectively, while the population of the π^*(DAB) orbital increases by 0.2 electrons. This strikingly small extent of electron redistribution on $\sigma \rightarrow \pi^*$ excitation is caused by an exceptionally strong mixing between the axial Sn–Ru–Sn σ orbital and the π^*(DAB) orbital both in the ground and excited state, as was discussed earlier. The concomitant mixing between the Ru-5d_{yz} and π^*(DAB) orbitals in the LUMO further diminishes the charge separation in the $\sigma\pi^*$ excited state through compensating changes of the Ru-DAB π bonding. The Ru-5d_{yz} population was actually calculated to increase on $\sigma\pi^*$ excitation by 0.07 electrons.

The photophysical and photochemical behaviour of $Ru(SnPh_3)_2(CO)_2$(*i*Pr-DAB) indeed reflect the small structural effects of the $\sigma\pi^*$ excitation predicted by the theoretical considerations [72]. Characteristically, the emission from the $^3\sigma\pi^*$ excited state measured in a low-temperature glass is very long lived (264 μs), despite its low energy. The apparent Stokes shift is rather small. Long-lived (ca. 1 μs) emission was even observed at r.t. in a fluid solution. The temperature dependence of the emission lifetime measured [72] in a fluid THF solution follows an Arrhenius-type behaviour (Eq. (2)). The intrinsic non-radiative decay by weak coupling to the

ground state is very slow, $k_0 = 3.1 \times 10^4$ s^{-1}. This value is about 10–100 times smaller than that of MLCT or LLCT excited states of Re or Ru complexes. The thermally activated decay pathway occurs with $A = 3.9 \times 10^8$ s^{-1}, over an energy barrier of $E_a = 1470$ cm^{-1}. Irradiation of $Ru(SnPh_3)_2(CO)_2$(*i*Pr-DAB) with visible light produces $Ph_3Sn^{\cdot}$ and $Ru(SnPh_3)(CO)_2$(*i*Pr-DAB)$^{\cdot}$ radicals with a quantum yield of 0.23 at 290 K [75]. The temperature dependence of the photochemical quantum yield, $\phi = \phi_0 \exp(-E'_a/RT)$, holds the key to the understanding of the $Ru(SnPh_3)_2(CO)_2$(*i*Pr-DAB) photochemistry [75]. The value of the photochemical activation energy E'_a is identical to the activation energy of the non-radiative excited state decay. It follows that the emitting $^3\sigma\pi^*$ state of $Ru(SnPh_3)_2(CO)_2$(*i*Pr-DAB) is intrinsically stable and the Ru–Sn bond homolysis occurs via a higher lying excited state, presumably of a $\sigma\sigma^*$ origin. This situation is shown schematically in Fig. 13.

Time-resolved spectra of $Ru(SnPh_3)_2(CO)_2$(*i*Pr-DAB) exhibit [72] features characteristic of the $^3\sigma\pi^*$ excited state absorption, see Fig. 14. Neither the spectral pattern, nor the excited state lifetime, which is identical with the emission lifetime, depends on the solvent, THF or hexane. The profoundly different patterns of the excited state absorption spectra of the $\sigma\pi^*$ and LLCT states become apparent upon comparison of the time-resolved spectra of $Ru(SnPh_3)_2(CO)_2$(*i*Pr-DAB) and $Ru(SnPh_3)(Cl)(CO)_2$(*i*Pr-DAB), respectively, Fig. 14. More detailed structural information on the lowest excited state of $Ru(SnPh_3)_2(CO)_2$(*i*Pr-DAB) came from the TR-IR spectra [72] measured in PrCN glasses at 77 K, see Fig. 15. Again, a comparison with the spectra of the LLCT-excited $Ru(SnPh_3)(Cl)(CO)_2$(*i*Pr-DAB) is especially revealing. While the LLCT excitation still shifts the ν(CO) bands to

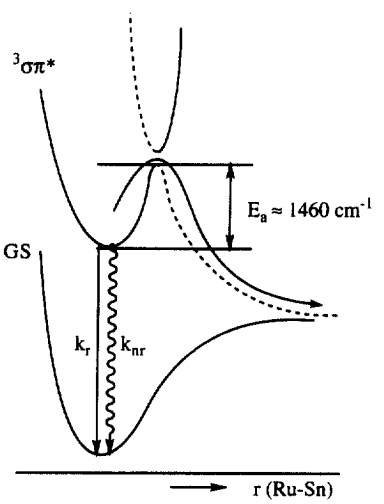

Fig. 13. Dynamics of the $^3\sigma\pi^*$ excited state of $Ru(SnPh_3)_2(CO)_2$(*i*Pr-DAB). The decay mechanism involves emission, k_r, non-radiative deactivation by weak coupling to the ground state, k_{nr}, and a thermally activated conversion to a dissociative state (dashed curve) which ultimately leads to Ru–Sn bond homolysis [75].

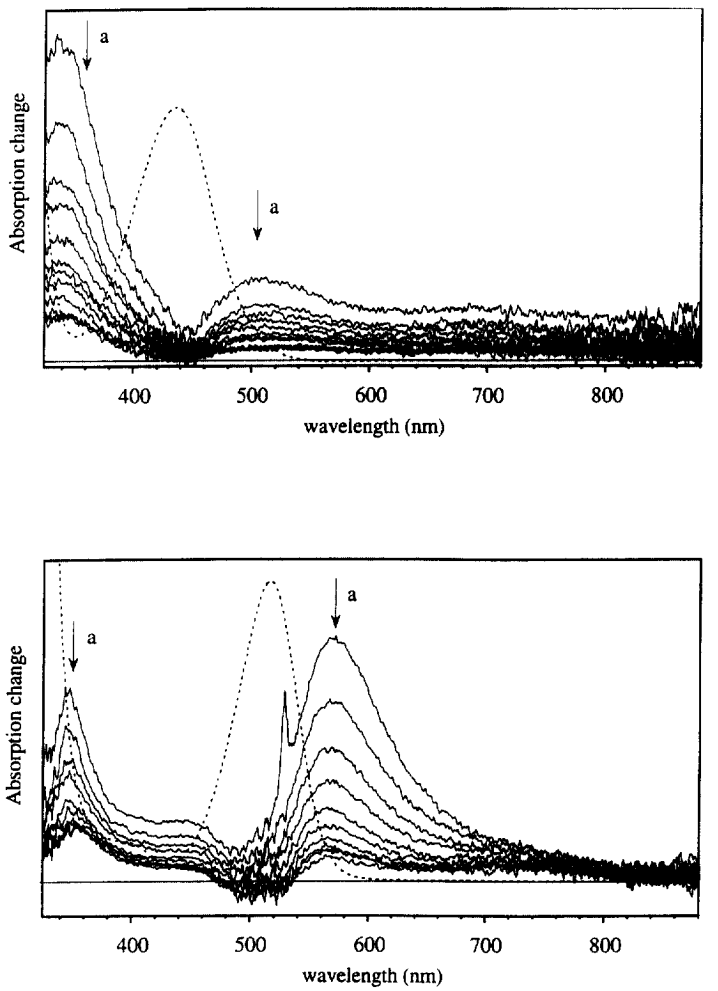

Fig. 14. Excited state visible absorption spectra of $Ru(Cl)(SnPh_3)(CO)_2(i$Pr-DAB), top, and $Ru(SnPh_3)_2(CO)_2(i$Pr-DAB), bottom, measured in THF at r.t. [72]. ↓a points to the decaying transient absorption. Delay between measurements of individual spectra: 200 ns, top; 300 ns, bottom. Ground state spectra are shown as dashed curves.

higher wavenumbers, albeit by a small amount, no such shift was found for the $^3\sigma\pi^*$ state of $Ru(SnPh_3)_2(CO)_2(i$Pr-DAB). The frequency of its ν(CO) band at 2006 cm^{-1} does not change on excitation at all while the ν(CO) band at 1955 cm^{-1} shifts by 11 cm^{-1} to lower wavenumbers. This corresponds to a relatively insignificant decrease of the CO stretching force constant by some 8 N m^{-1}. Obviously, the Ru→CO π back donation, and hence, the electron density on the Ru atom is virtually unchanged by $^3\sigma\pi^*$ excitation, in accord with the results of the DFT-MO calculations, vide supra.

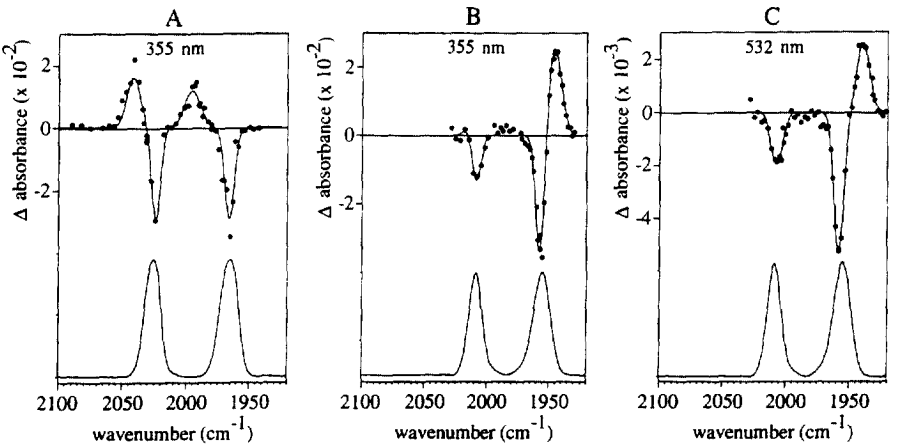

Fig. 15. Excited state IR absorption spectra of $Ru(Cl)(SnPh_3)(CO)_2(i$Pr-DAB) (A) and $Ru(SnPh_3)_2(CO)_2(i$Pr-DAB) (B, C), obtained from 77 K in *n*PrCN glass at 120 ns after 355 or 532 nm laser excitation [72]. Ground state FTIR spectra are shown below.

The photochemical [75] and photophysical [72] behaviour of other Ru complexes with chemically identical or similar axial ligands, $Ru(PbPh_3)_2(CO)_2(i$Pr-DAB), $Ru(SnPh)_3(GePh_3)(CO)_2(i$Pr-DAB), or $Ru(SnPh_3)(SnMe_3)(CO)_2(i$Pr-DAB) resembles that of $Ru(SnPh_3)_2(CO)_2(i$Pr-DAB), although the respective $^3\sigma\pi^*$ lifetimes are shorter [72,75].

The photochemistry of $Re(Me)(CO)_3(\alpha$-diimine) complexes is exceptional [54,57,60,61]. Although the Re–Me bond homolysis occurs on a femtosecond timescale [57,132], the quantum yields are rather low and temperature dependent. A strong dependence on the excitation wavelength was found for *i*Pr-Pyca and

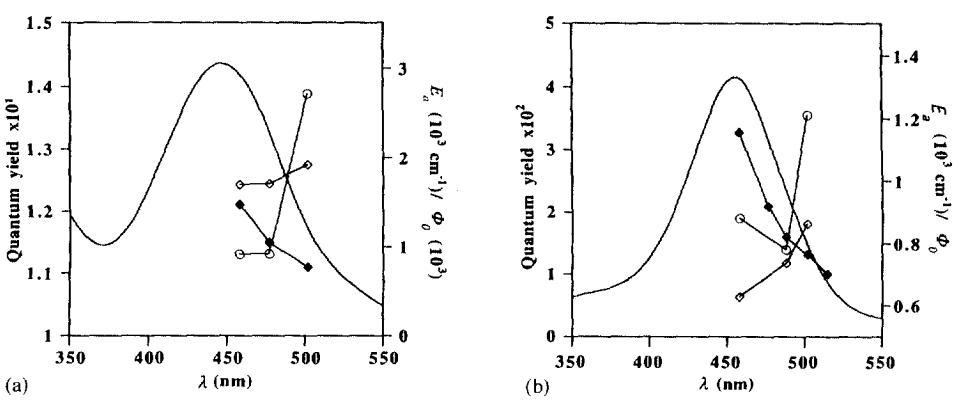

Fig. 16. Ground state absorption spectra and excitation wavelength dependence of the photochemical quantum yield (at 273 K in THF), ◆; activation energy E_a, ◇; and preexponential factor ϕ_0, ○; measured in THF for: (a) $Re(Me)(CO)_3(i$Pr-PyCa); and (b) $Re(Me)(CO)_3(i$Pr-DAB) [54,57].

*i*Pr-DAB, see Fig. 16. The optical excitation is followed by two parallel deactivation pathways: a prompt Re–Me bond homolysis via a $^3\sigma\pi^*$ excited state and a relaxation through a long-lived ^{3}MLCT state. The dissociative $^3\sigma\pi^*$ state lies above the initially excited ^{1}MLCT state from which it is populated by a temperature-dependent strong-coupling mechanism. The unreacted fraction of the initially excited molecules decays through the ^{3}MLCT state, which was indeed detected by a time-resolved absorption spectroscopy and, for Re(Me)(CO)$_3$(bpy′), also by emission. It has been conclusively demonstrated that the ^{3}MLCT state is not involved in the Re–Me homolysis [60].

The remarkable sensitivity of the photochemical reactivity of Re(R)(CO)$_3$(α-diimine) and Ru(R)(E′)(CO)$_2$(α-diimine) complexes toward the nature of the alkyl ligand R emphasises the delicate balance between excited states of a different orbital origin and distinct properties, which is controlled by small variations in the axial ligand. The difference between the Re–Me and Re–Et σ-bonding or even between the Ru–C and Ru–*i*Pr bonds is enough to switch the relative order of MLCT and $\sigma\pi^*$ states. The M–Me σ-bonding orbital is stabilised relative to the M–Et or M–*i*Pr σ orbital by a better overlap between the methyl carbon sp^3 and the metal d_{z^2} orbitals [134,135]. Hence, the M–Me σ orbital lies [116] below the d_π orbital and the $\sigma\pi^*$ state is placed above the MLCT state, see Fig. 12. The alkyl effects on the relative ordering of the $\sigma\pi^*$ and MLCT states was well reproduced by CASSCF/CCI calculations [134] on Mn(R)(CO)$_3$(H-DAB) (R = H, Me, Et) and by DFT-MO calculation on Ru(R)(Cl)(CO)$_2$(H-DAB) (R = Me, *i*Pr) model complexes [128].

Whereas it is well-established that the axial metal–ligand bond homolysis of the dinuclear and alkyl complexes and the long-lived, low-energy, emission of the former species originate in a $^3\sigma\pi^*$ excited state, the nature of the electronic transition responsible for their visible absorption band is less clear. Most of the dinuclear and alkyl complexes exhibit a single visible absorption band that shows all the features characteristic of CT excitations: high intensity, broad and structureless shape, solvatochromism, rigidochromism. Originally, the visible absorption band of the metal–metal bonded complexes Re(E)(CO)$_3$(α-diimine) [E = SnPh$_3$, Mn(CO)$_5$, Re(CO)$_5$; diimine = phen, bpy] was attributed [3,62] to the spin- and symmetry-allowed $\sigma \rightarrow \pi^*$ transition. This assignment was based on the considerations of d_π and σ orbital energies estimated from photoelectron spectra. Later, it was pointed out [46,109,136,137] that the Raman spectra measured in resonance with the lowest absorption band of Re(SnPh$_3$)(CO)$_3$(*t*Bu-DAB), Re(Mn(CO)$_5$)(CO)$_3$(*i*Pr-DAB) or Re(Re(CO)$_5$)(CO)$_3$(*i*Pr-DAB), show a strong enhancement of the band due to the ν_s(CN) and, except for the last species, of the ν_s(CO) band. Analogous rR spectrum was obtained for Re(Me)(CO)$_3$(α-diimine) species [61,116]. These rR features indicate a predominant (Re → DAB) MLCT character of the resonant electronic transition. Raman peaks due to the ν(Re–E) vibration, which were expected to be strongly enhanced by resonance with the $\sigma \rightarrow \pi^*$ transition, are very weak, if present at all. Hence, the lowest absorption band of the dinuclear and alkyl complexes was attributed to one or more MLCT transitions. However, the CASSCF/CCI calculations [138,139] on the Re(H)(CO)$_3$(H-DAB)

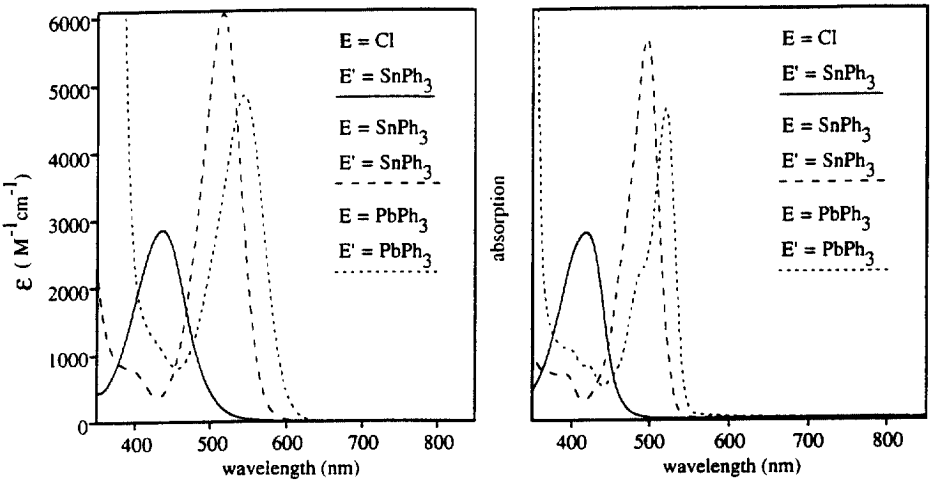

Fig. 17. Visible absorption spectra of Ru(E)(E')$(CO)_2$(*i*Pr-DAB) complexes measured at 293 K in THF (left) or at 77 K in a 2-Me–THF glass (right) [79].

model molecule suggest a strongly mixed MLCT/$\sigma\pi^*$ character of the lowest allowed electronic transition. In conclusion, it appears that the optical excitation of the Re(E)$(CO)_3$(diimine) complexes containing covalent Re–C or Re–metal bond leads to a mixed ^{1}MLCT/$\sigma\pi*$ Franck–Condon excited state which undergoes a very fast non-radiative conversion into the $^3\sigma\pi^*$ state. The extent of the MLCT–$\sigma\pi^*$ mixing probably depends on the diimine and axial ligands and, perhaps, also on the solvent. It does not occur in analogous Mn complexes whose Franck–Condon state appears to be of a pure MLCT character.

Unlike their Re counterparts, the Ru complexes show a profound change in the ground-state absorption and rR spectra on going from the Ru(E)(X)$(CO)_2$(α-diimine) (X = Cl, Br, I) complexes with a MLCT or LLCT lowest excited state to Ru(E)(E')$(CO)_2$(*i*Pr-DAB) (E,E' ≠ halide) species with a lowest $\sigma\pi^*$ state [72]. Notably, the lowest absorption band shifts by some 80 nm to the red, its molar absorptivity rises about twice, solvatochromism decreases, ν(CO) and ν(CN) frequencies drop by some 20 and 70 cm^{-1}, respectively. At the same time, the rR spectral pattern changes completely. The rR spectra of the Ru(E)(X)$(CO)_2$(σ-diimine) (X = Cl, Br, I) species are dominated by the peak due to the ν_s(CN) vibration, indicating a highly localised character of the MLCT/LLCT resonant transition. On the other hand, rR spectra of Ru(E)(E')$(CO)_2$(α-diimine) (E,E' ≠ halide) complexes show many weak peaks that belong to ν_s(CN), ν(CC) and deformation vibrations of the DAB ligand and to the low-wavenumber vibrations of the Ru(DAB) chelate ring [72,74,79,83]. These changes in spectroscopic properties are demonstrated in Figs. 17 and 18 by comparing the spectra of the Ru$(SnPh_3)$(Cl)$(CO)_2$(*i*Pr-DAB) and Ru$(SnPh_3)_2(CO)_2$(*i*Pr-DAB) complexes. The spectral features of the complexes with both axial ligands bound covalently (E,E' ≠ halide) may be accounted for by the mixing between the axial σ and

π^*(diimine) orbitals. This $\sigma-\pi^*$ delocalisation, which was extensively discussed above, removes any overlap restrictions on the $\sigma \rightarrow \pi^*$ electronic transition which then manifests itself by a strong visible absorption band. The relative sharpness of this band is in line with the small molecular distortion on $\sigma \rightarrow \pi^*$ excitation. The rR spectra also show that the excited state distortion is weak, distributed over many normal coordinates. The $\sigma \rightarrow \pi^*$ character of the lowest allowed electronic transition was well reproduced [72,74,82] by DFT-MO calculations on several model molecules: $Ru(E)(SnH_3)(CO)_2$(H-DAB) (E = SnH_3, Me); $Ru(E)[Mn(CO)_5](CO)_2$(H-DAB) (E = Me, $Mn(CO)_5$); or $Ru(i\text{Pr})(I)(CO)_2$(H-DAB). These calculations have even

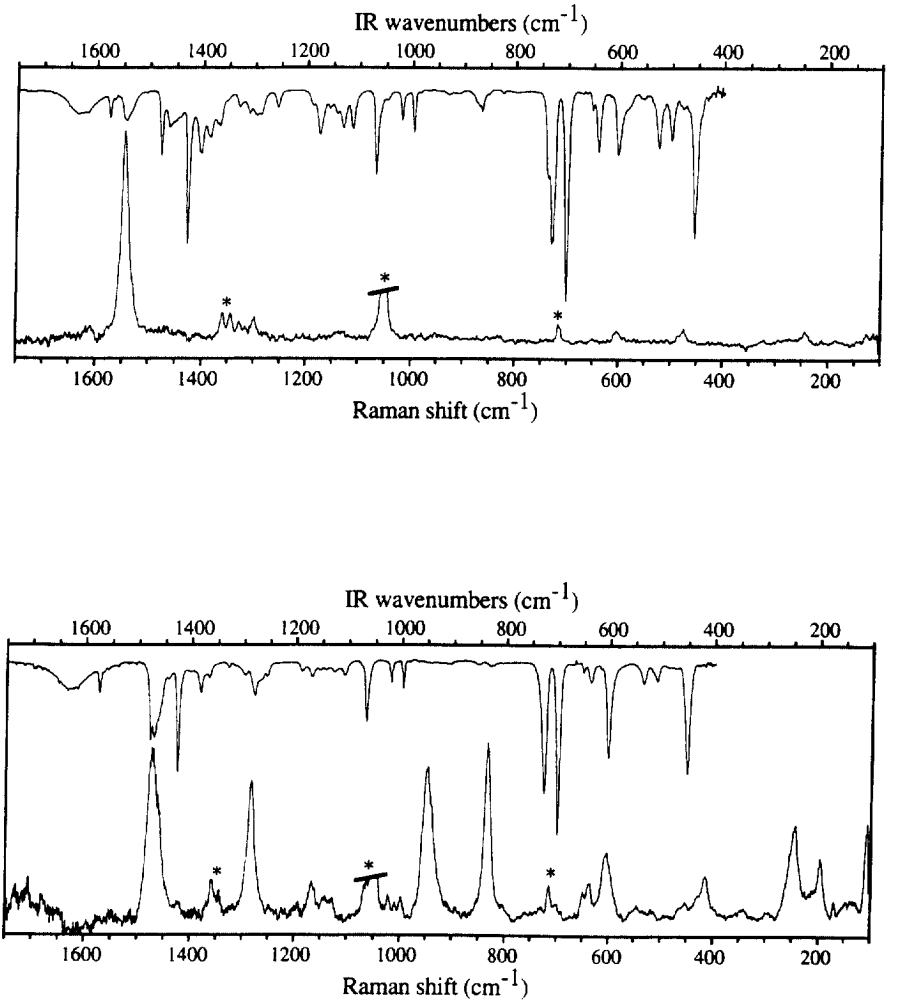

Fig. 18. IR and resonance Raman spectra of $Ru(SnPh_3)(Cl)(CO)_2(i\text{Pr-DAB})$, top, and $Ru(SnPh_3)_2(CO)_2(i\text{Pr-DAB})$, bottom. IR and rR spectra were obtained from KBr or KNO_3 pellets, respectively [72].

indicated that the oscillator strength of the $\sigma \rightarrow \pi^*$ transition is larger than that of the higher lying MLCT one. The calculated trends in transition energies and relative intensities agree well with the experimental spectra.

4. Effects of the α-diimine ligand

4.1. Relations between the diimine structure and properties of charge-transfer states

The particular character of the lowest excited state—MLCT, LLCT, or $\sigma\pi^*$—is largely determined by the structure of the $Re(E)(CO)_3$ or $Ru(E)(E')(CO)_2$ fragments in which the excited electron originates. However, all the different types of charge-transfer states are introduced into organometallic molecules by an electron accepting ligand, most often an α-diimine, which possesses a low-lying, unoccupied π^* orbital. This is the terminal orbital for all the charge-transfer excitations, regardless of their particular character. Hence, variations in the structure of the diimine ligand affects profoundly the properties of the CT states, namely their energy, emission quantum yield, lifetime, mechanism of non-radiative deactivation, and reactivity.

The energy of the π^*(diimine) orbital is the crucial factor since it determines the energy of the CT excited states and the extent of the metal→diimine π back bonding. In general, reduction potentials [25–27,80,93] of $Re(E)(CO)_3$(α-diimine) complexes and of the free ligands indicate that the π^* orbital energy decreases in the approximate order:

$$\text{phen, bpy} > \text{R-PyCa} > \text{dpp} > \text{R-DAB, bpym} > \text{dpq} > \text{Ar-DAB}, \tag{10}$$

while the Re→diimine π back bonding in the same order strengthens:

$$\text{phen, bpy} < \text{R-PyCa} < \text{dpp} < \text{bpym} \leq \text{dpq} \leq \text{R-DAB} < \text{Ar-DAB}. \tag{11}$$

The R-DAB ligands are somewhat stronger π-acceptors than aromatic diimines of comparable π^* orbital energy like dpp, bpym or dpq. This is caused by a larger contribution from the N-$2p_z$ orbitals to the π^* orbital of the DAB ligands, which, in turn, results in a larger d_π-π^* overlap. The absorption and emission energies of $Re(E)(CO)_3$(α-diimine) and $Ru(E)(E')(CO)_2$(α-diimine) complexes decrease as a function of the diimine ligand in the order of decreasing π^* orbital energies (Eq. (10)). Eqs. (10) and (11) are also supported by the results of quantum chemical studies [128,140].

Essentially, the dependence of the non-radiative decay rate on the structure of the diimine ligand follows the energy gap law, EGL, as formulated in Eq. (4). However, a simple linear increase of the decay rate with decreasing emission energy could only be observed in series of complexes whose diimine ligands are structurally very similar. The best examples are the $Re(Cl)(CO)_3(4,4'\text{-}X_2\text{-bpy})$ or $Re(4Et\text{-}py)(CO)_3(4,4'\text{-}X_2\text{-bpy})^+$ series for which excellent EGL correlations were found [8,37]. A similar EGL correlation has also been determined [94] for the $Re(4Et\text{-}py)(CO)_3(4,4'\text{-}X_2\text{-}5,5'\text{-}Y_2\text{-bpy})$ series, for which both the emission energy and k_{nr}

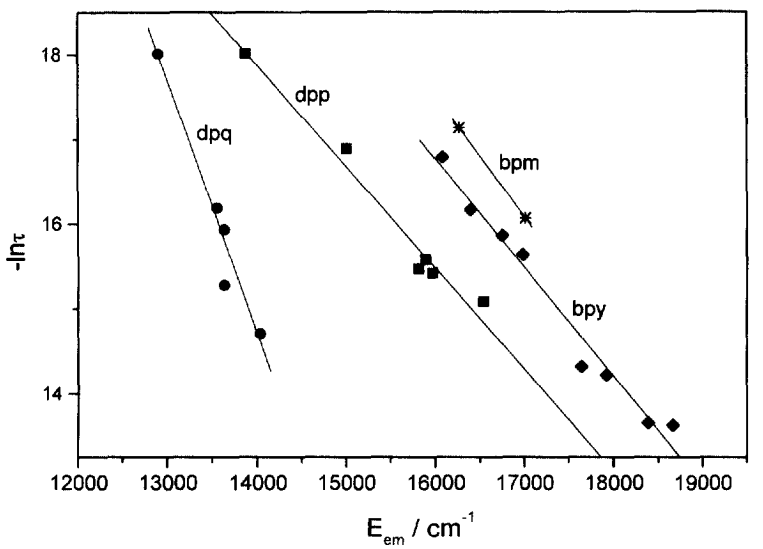

Fig. 19. EGL map for Re(E)$(CO)_3$(α-diimine) complexes with different diimine ligands. Data from Refs. [6,8,93,127].

were also correlated with the Hammet constants of the substituents X and Y. Decay of the $[Re(py\text{-}PTZ^{\bullet+})(CO)_3(4,4'\text{-}X_2\text{-}bpy^{\bullet-})]^+$ LLCT state also follows the EGL [37].

Based on EGL, one would expect that the non-radiative decay rate will increase as a function of the diimine ligand (other structural factors and the medium being constant) with decreasing π^* orbital energy in the order of 10. However, structural differences between various diimine ligands are too large to allow for such a simple correlation. For example, EGL maps in Figs. 2 and 3 show that, although the increase in ln k_{nr} in the order bpy < *i*Pr-PyCa < *i*Pr-DAB parallels the decrease in E_{em}, the decay rate observed for the DAB complexes is much larger than expected, at least for the MLCT and LLCT states. Also, despite comparable emission energies, phen complexes show consistently slower decay rates of both MLCT [89] and $\sigma\pi^*$ [62] states than their bpy counterparts. Fig. 19 compares EGL plots obtained for series of Re(E)$(CO)_3$(α-diimine) complexes (α-diimine = bpy, dpp, dpq, or bpm) in which the emission energy is varied by changing the axial ligand X. It is obvious that, at comparable emission energies, the non-radiative decay rate would decrease in the order bpm > bpy > dpp > dpq. Moreover, the EGL plots have very different slopes and intercepts. The dependence of the decay rate on the diimine structure that is not paralleled by corresponding changes in the emission energy generally results from the following factors which are all strongly diimine-dependent: (i) excited state distortion S_m; (ii) mean frequency of the acceptor vibrations ω_m; (iii) electronic coupling between the ground and excited state; (iv) coupling to solvent; (v) energy difference from higher, rapidly decaying states; and (vi) excited state reactivity. These factors will now be discussed individually.

Decreasing excited state distortion diminishes the vibrational overlap with the energy-accepting vibrational levels of the electronic ground state, slowing down the non-radiative decay. Excited state distortion often increases with increasing excited state energy. This effect was found already in the 'well behaved' $Re(Cl)(CO)_3(4,4'\text{-}X_2\text{-bpy})$ series [8]. It was explained by a larger charge separation in more energetic MLCT states which, thus, decay somewhat faster than expected from EGL.

On the other hand, delocalisation of the π^* orbital over a large, rigid, diimine ligand backbone severely limits distortion of CT excited states [89,91]. This is clearly manifested by a decrease of the decay rate on going from bpy to the more rigid and delocalised phen and, especially, by the effect of increasing the delocalisation by annealing benzene rings to the dpp ligand. The decay rate decreases in the order dpp > dpq > dpb, as was observed for many Re carbonyl complexes [93] as well as for Ru^{II} and Os^{II} polypyridyl complexes [89,91]. The effect of the delocalisation of the π^* orbital on the MLCT excited state distortion is reflected [93] by the drop of the S_m value from 1.12 to 0.11 on going from $Re(E)(CO)_3(dpp)^{0/+}$ to $Re(E)(CO)_3(dpq)^{0/+}$. Increasing the delocalisation of the electron-accepting π^* orbital over the diimine ligand effectively means that the structural effects of the CT excitation are distributed over a larger number of bonds, each being affected only a little. Such a delocalised excitation may activate not only the usual ν(CN) and ν(CC) diimine acceptor vibrations, but also deformation vibrations of the diimine ligand which occur at lower frequencies. This is nicely demonstrated by the $Re(E)(CO)_3(dpp)^{0/+}$ and $Re(E)(CO)_3(dpq)^{0/+}$ complexes [93]: resonance Raman spectra of the dpp species show that the vibrations in the frequency range of 1250–1650 cm^{-1} are the most effective acceptors. However, the deformation vibrations at 740 and 815 cm^{-1} were found to be strongly activated for the more delocalised dpq complexes. Accordingly, the average acceptor frequency $\hbar\omega_m$ decreases from 1379 to 1157 cm^{-1} on going from the dpp to the dpq species. This decrease in the frequency of the acceptor vibrations further slows down the non-radiative decay since the low-frequency vibrations are less effective energy acceptors. Inspection of Eq. (4) shows that lower values of $\hbar\omega_m$ mean more negative slopes of EGL correlations. This is in accord with the very high sensitivity of the decay rate of MLCT-excited $Re(E)(CO)_3(dpq)^{0/+}$ complexes toward the excited state energy, see Fig. 19.

Changing the diimine ligand from bpy′ to R-PyCa and R-DAB is accompanied by an increase in excited state distortion, manifested by increasing apparent Stokes shift. This is caused by increasing flexibility and, namely, diminishing the ligand framework over which the excited electron may be delocalised. Accordingly, the decay rates of many Re and Ru carbonyl–DAB complexes are larger than expected from EGL (Figs. 2 and 3).

An electronic coupling between the excited and ground states is expected to increase with increasing metal→diimine π back bonding following the order 11. Metal–ligand π interaction mixes the d_π and π^*(diimine) orbitals, resulting in $(d_\pi + \pi^*)$ and $(d_\pi - \pi^*)$ orbitals which are π-bonding and antibonding, respectively, toward the M–N(diimine) bonds [109]. As the metal–ligand interaction in a series of complexes with different diimine ligands strengthens, the charge separation in the

excited state diminishes and the excitation becomes partially delocalised over the whole M(diimine) chelate ring. Such a situation manifests itself by increasing oscillator strength of the CT absorption band and decreasing solvatochromism on going from bpy′ to *i*Pr-PyCa, R-DAB and to Ar-DAB [109,141]. These trends were found for $Re(E)(CO)_3(\alpha\text{-diimine})$ complexes regardless of the nature of the axial ligand, E = halide, metal fragment or alkyl. The π back bonding is always the largest for the DAB ligands, both because of a relatively low π^* orbital energy and a large $\pi^*\text{–}d_\pi$ overlap. Vibronic coupling between the ground and excited state is more efficient in complexes with strong M–N(diimine) π interaction [141] since the low-frequency ν(M–N) promoting vibrations (ω_k, Eqs. (6) and (7)) readily change the overlap between the d_π and π^*(diimine) orbitals, thus removing the orthogonality of the two electronic states. Increasing strength of the Re → diimine π back bonding is another important factor that contributes to an increase of the CT excited state decay rate in the order bpy′ < RPyCa < R-DAB < Ar-DAB. Electronic coupling also seems to increase on going from $Re(E)(CO)_3(dpp)^{0/+}$ to $Re(E)(CO)_3(dpq)^{0/+}$ complexes. This is indicated by the intercept of their respective EGL correlations [93], which is much larger (58.7) for the dpq series than for the dpp one (35.1). So far, no systematic studies of the electronic coupling between the CT states and the ground state and of its structural dependence have been carried out.

Other diimine-dependent factors that influence the behaviour of the CT states appear to be less important than the effects of excited state distortion and electronic coupling. No strong diimine-dependent solvent effects were noticed, with the possible exception [127] of monomolecular $Re(E)(CO)_3(bpm)^+$; E = py, CH_3CN; complexes which show much shorter MLCT lifetimes in CH_3CN than in CH_2Cl_2. Variations in the energy difference from higher, rapidly decaying states, is of a little importance for the complexes discussed herein. However, the proximity of IL excited states may affect photophysical behaviour for some diimine ligands, especially phen derivatives or dppz, vide infra.

To summarise, the structure of the diimine ligand affects the properties of the CT states (MLCT, LLCT, $\sigma\pi^*$) of Re and Ru carbonyl–diimine complexes through the energy of the accepting π^*(diimine) orbital, its delocalisation over the diimine ligand framework and by the extent of its interaction with the metal d_π orbital. An increase of the π^* orbital energy slows down the non-radiative decay. Increasing delocalisation of the excited electron over a large, preferentially rigid, diimine ligand framework restricts the excited state distortion. This may be accompanied by a decrease in the mean frequency of the acceptor vibrations. Both these effects strongly diminish the non-radiative decay rate of the CT states. On the other hand, an increase of the M → diimine π back bonding strengthens the electronic coupling between the excited and ground state, facilitating the non-radiative decay. For the complexes discussed herein, the rate of the non-radiative decay generally increases (excited state lifetime decreases) according to the order 11, particularly bpy < R-PyCa < R-DAB < Ar-DAB. On the other hand, the rate of radiative decay generally decreases in the order 10: bpy > R-PyCa > RDAB > Ar-DAB. The combination of these two effects leads to a decrease of emission quantum yields on going from bpy to the PyCa and to DAB ligands.

4.2. Intraligand (α-diimine) excited states

Charge transfer states are not the only low-lying excited states produced by exciting an electron into the π^*(diimine) orbital. In fact, some diimine ligands possess low lying intraligand, IL, excited states of a $\pi \rightarrow \pi^*$ character in which the electron is excited from a predominantly diimine-localised occupied π-bonding orbital. The nature of the lowest excited state of complexes of such ligands is then determined by the relative energy of the CT and IL excited states which depends not only on the diimine ligand, but also on the metal, the axial ligand(s) and even on the temperature and/or the medium.

Experimentally, the IL character of the emissive excited state is manifested by a sharp, structured, emission band which resembles that of the free ligand. The ^{3}IL states are usually rather long-lived, although their lifetimes are shorter compared with the free ligands. Lifetimes of the ^{3}IL emission often exhibit complicated temperature dependencies because their decay may involve close-lying states of other orbital origin. It should be noted that the observation of a typical broad MLCT emission from a complex with close-lying MLCT and IL states does not necessarily prove that MLCT is the lowest state. This is the case of $Re(Cl)(CO)_3(dppz)$ at r.t. in a fluid solution [142]. The character of its lowest excited state was determined by time-resolved resonance Raman spectroscopy to be $\pi \rightarrow \pi^*$ IL. However, both its radiative and non-radiative decay to the ground state are rather slow. Instead of decaying directly to the ground state, the ^{3}IL state of $Re(Cl)(CO)_3(dppz)$ is deactivated through a higher lying, emissive, MLCT state that is close in energy. Hence, only the MLCT emission is observed. On the other hand, both the emission and time-resolved Raman spectra of an analogous $Re(PPh)_3(CO)_3(dppz)^+$ complex point to an IL character of its lowest excited state [142]. Apparently, the MLCT state is, in this case, too high above the IL one to provide an efficient deactivation pathway. Emission spectra of several cationic complexes $Re(E)(CO)_3(R\text{-phen})^+$; R-phen = substituted phenanthroline derivatives; exhibit overlapping emission bands due to MLCT and IL emissions [143]. Their close lying MLCT and IL states are in thermal equilibria at ambient temperatures, whereas dual emission with a biexponential (or multiexponential) decay from non-equilibrated populations of IL and MLCT states was often observed for these complexes in low-temperature glasses [16,92,96,143,144].

A lowest intraligand excited state is common in cationic Re complexes of diimine ligands which possess an extensively delocalised π system, for example derivatives of phen, large aromatic ligands like dppz, dppn, or for DAB or PyCA ligands with aromatic substituents on their N-donor atoms. While the energy of the IL state is largely determined by the diimine ligand, the variable energy of the CT state makes the relative ordering of the IL and CT states strongly structure- and medium-sensitive. In general, the occurrence of an IL lowest state in $Re(E)(CO)_3(\alpha\text{-diimine})^{0/+}$ complexes is favoured by the presence of weakly σ-donating and strongly π-accepting axial ligands, for example phosphines, phosphites, nitriles, or isonitriles, which push the CT states up in energy. The energy of the CT state also increases on going from fluid solutions to rigid media like polymer matrices, crystals or low-tempera-

ture glasses while the IL states are virtually unaffected since they do not involve a charge separation. If the rigidochromic effect is larger than the separation between the lower lying CT state and the IL state, their relative ordering may be altered by changing the medium. Thus, many $Re(py\text{-}X)(CO)_3(R\text{-}phen)^+$; py-X = pyridine derivatives; or $Re(CH_3CN)(CO)_3(R\text{-}phen)^+$ complexes show broad, structureless MLCT emission from fluid solutions while a highly structured long lived IL emission is observed from low-temperature glasses [46,92,96,143,144]. Strongly π-accepting isonitrile ligands in the axial position push the MLCT states to still higher energy. Hence, $Re(CN\text{-}t\text{Bu})(CO)_3(R\text{-}phen)^+$ complexes exhibit either pure IL emission or mixed IL/MLCT emission even from room temperature CH_2Cl_2 solutions [16].

The $Re(CO)_4(bpy)^+$ complex with two axial CO ligands presents an extreme case. The MLCT states are so high in energy that the emission occurs from an ^{3}IL(bpy) state in rigid media as well as in fluid solutions [119–122]. Notably, this is the only known Re carbonyl–bipyridine complex whose lowest excited state has an IL character. Detailed analysis of the emission and absorption spectra obtained from single crystals and PMMA glasses at cryogenic temperatures has revealed [121] that 3% of a ^{1}MLCT character is admixed into the emissive ^{3}IL state by spin–orbit coupling. Importantly, this, relatively small, ^{1}MLCT admixture has profound photophysical effects. It increases the oscillator strength of the transition to the ^{3}IL state, changes its polarisation, increases the S_m factor, and shortens the emission lifetime by five orders of magnitude relative to free bpy. It is interesting to note that the ^{1}MLCT admixture is only 1% for the closely related $Re(CO)_4(phen)^+$ complex due to a much smaller spin–orbit matrix element, 65 cm^{-1}, as compared with 261 cm^{-1} for $Re(CO)_4(bpy)^+$.

4.3. Complexes with non-diimine acceptor ligands

The remarkable ability of α-diimines to introduce long-lived, emissive, and/or reactive charge transfer excited states into organometallic molecules of low-valent metals seems to originate in a unique balance of the energy and (de)localisation of their lowest unoccupied π^* orbital, and the extent of its electronic interaction with the metal d_π orbitals together with a relatively small structural distortion of the diimine ligand on accepting the excited electron. Although α-diimines are the most common ligands which give rise to charge transfer excited states, other electron-acceptors with low-lying unoccupied π^* orbitals may also form organometallic complexes exhibiting intriguing CT excited state properties.

$Re(Cl)(CO)_3(L)_2$ complexes in which L is a monodentate pyridine derivative have long-lived MLCT excited states whose behaviour is very similar to that of $Re(Cl)(CO)_3(bpy)$ and its analogues. The MLCT excited state of $Re(Cl)(CO)_3(4,4'\text{-}bpy)_2$ was the first one to be characterised by TRIR spectroscopy [145]. Typical high-frequency shifts of ν(CO) bands were observed and used in a vibrational analysis of the MLCT state within the CO energy-factored force field approximation [115]. $Re(Cl)(CO)_3(L)_2$ complexes, in which L = 4-Ph-pyridine, 4-NC-pyridine, quinoline or isoquinoline, have a lowest MLCT or IL excited state [146–149],

depending on L and the medium. Their photophysical behaviour resembles that of the phen complexes. Obviously, the occurrence of long-lived emissive excited states is not restricted to complexes with chelated acceptor ligands. Some of these species undergo an interesting photoreactivity under UV irradiation that was attributed to a higher $Re(Cl)(CO)_3(L^{\cdot -})(L^{\cdot +})$ LLCT state [146,147,149].

An interesting excited state behaviour is also exhibited by Re complexes with chelated dithiooxamide ligands, DTO [150,151]. The $Re(Br)(CO)_3(DTO)$ complex shows absorption bands in the visible spectral region which belong to transitions of a mixed (Re→DTO) MLCT/(Br→DTO) LLCT character. By contrast to its photostable diimine analogues, visible light irradiation of $Re(Br)(CO)_3(DTO)$ leads to a photochemical substitution of the axial Br ligand by $P(n\text{Bu})_3$ following an associative mechanism, while UV irradiation results in a CO loss [151].

Oxygen-coordinated ligands also form complexes with low lying MLCT states. Complexes of the type $Re(CO)_{4-n}(L)_n(DBSQ)$ (DBSQ = 3,5-di-*t*butyl-1,2-benzosemiquinone radical anion, L = various Lewis bases, $n = 0$, 1, 2) show typical MLCT absorption bands in the visible spectral region. Delocalisation of the corresponding MLCT transition over the Re(DBSQ) chelate ring increases with increasing Lewis basicity and the number of the co-ligands L [152,153]. Ligand-localised oxidation produces complexes $Re(CO)_{4-n}(L)_n(DBQ)^+$ (DBQ = 3,5-di-*t*butyl-1,2-benzoquinone) that contain the very strongly electron-accepting *o*-quinone ligand. Their low lying electronic transitions are completely delocalised over the Re(DBQ) chelate ring, as was revealed by rR spectroscopy [154]. Neither of the diimine ligands discussed in the preceding sections is as strong a π-acceptor as DBQ. The PhC(=O)C(=NR)Ph ligand, abbreviated (N,O), forms $Re(X)(CO)_3(N,O)$; X = Cl, I; complexes which are characterised by a low-energy absorption band attributed to a mixed MLCT/LLCT transition. This excitation appears to be largely delocalised over the Re(N,O) chelate ring [123]. Neither the photophysics nor the photochemistry of the Re complexes with oxygen-coordinated acceptor ligands have been studied.

N,C^--coordinated organometallic ligands are very promising electron acceptors which are known to form photoactive complexes with Pt^{II} and Ru^{II} [155]. The only known example of a Re complex is $Re(CO)_4(ppy)$, which contains the anion of 2-Ph-pyridine, ppy, coordinated through the N and C^- atom of the pyridine and phenyl ring, respectively. Its lowest excited state was determined to be ^{3}IL with a small ^{1}MLCT admixture [156]. The same lowest excited state was found for the N,S^--coordinated $Re(CO)_4$(2-(2-thienyl)pyridine) complex [157]. An interesting photophysical and photochemical behaviour is expected for Re–tricarbonyl complexes of these ligands with Lewis bases, halides or covalently bound ligands in the axial position. However, the synthesis of such complexes has still to be developed.

5. Ligand tuning of the excited state character: summary, perspectives and potential applications

As in most organometallic compounds of low-valent metals with electron-accepting

ligands, the MLCT excited state is very common in Re^{I} and Ru^{II} carbonyl–diimine complexes. It is the lowest excited state in those complexes in which the axial ligand is rather innocent, a conventional σ-donating Lewis base with neither strongly π donating nor π accepting properties. Intense MLCT emission and long lifetimes make such complexes promising luminophores or luminescence probes or sensors, especially in rigid media or confined supramolecular environments. The rate of their non-radiative decay follows the EGL behaviour when the axial ligand or substituents on the diimine ligand are varied. MLCT states in the $Re(E)(CO)_3(\alpha\text{-diimine})^{0/+}$ and $Ru(E)(E')(CO)_2(\alpha\text{-diimine})$ complexes are mostly stable toward ligand dissociation and their decay usually does not involve reactive LF states. The resulting photochemical stability makes these species promising sensitisers of electron transfer reactions. A much deeper understanding of the chemistry of their redox products, especially the oxidised forms, is necessary in order to utilise their excited state redox reactivity. Photoactive complexes that are chemically stable on oxidation and/or reduction are much needed.

Changing the axial ligand E to a π-donor (e.g. iodide) makes it possible to tune the character of the lowest excited state from MLCT to (E→diimine) LLCT through mixing between the occupied metal d_π orbitals and the p_π orbitals of the axial ligand. This orbital mixing and, hence, the relative contributions from the MLCT and LLCT characters to the lowest excited state are variable and strongly dependent on the axial ligand. Fine tuning of the excited state character may thus be achieved. The MLCT/LLCT change in the excited state character manifests itself by strong deviations from the EGL behaviour. The non-radiative decay rate drops on going from chlorides to iodides without a corresponding decrease in E_{em}. This appears to be caused by diminishing the excited state distortion and electronic coupling on going from MLCT to LLCT states. LLCT states may be populated by direct irradiation into absorption bands belonging to LLCT electronic transitions. Complexes with lowest LLCT states of this type are, again, photochemically rather stable, and, therefore, are suitable as redox sensitisers or luminophores. Despite somewhat smaller radiative decay rates, longer LLCT lifetimes may lead to larger emission quantum yields, as compared with pure MLCT emission.

Structural modifications of the axial ligands in complexes with a stable MLCT or LLCT lowest excited state can produce photoactive species with interesting applications. For example, attachment of a crown ether ring to axial pyridine ligands [17,18] could lead to sensors. Histidine [100], imidazole [23], or nucleobase [14] axial ligands give rise to Re complexes that can be specifically attached to proteins or other biomolecules and act as intramolecular photooxidants [23,44,45]. Bridging axial ligands give rise to polynuclear complexes capable of harvesting light energy [107,125]. Linking two $Re(CO)_3(bpy)$ moieties by acetylene groups aims at the development of molecular wires [98,99].

A different type of LLCT excited states, $Re(E^{\bullet+})(CO)_3(\alpha\text{-diimine}^{\bullet-})$, occurs in complexes whose axial ligand E may be oxidised by a net electron transfer. Such

LLCT states may be populated indirectly through higher-lying Re → diimine MLCT states. They are usually not emissive but the oxidised ligand $E^{\bullet +}$ may undergo chemical reactions. The possible synthetic or catalytic utility of these LLCT states remains to be explored.

Another type of CT excited state is introduced into the Ru or Re carbonyl–diimine complexes by axial ligands E with a high-lying σ-orbital, e.g. alkyls, benzyl, or metal-fragments like $SnPh_3$, $Mn(CO)_5$, $Re(CO)_5$, $CO(CO)_4$, etc. Such ligands form covalent M–E σ-bonds. The corresponding occupied σ-bonding orbital often lies above the d_π metal orbitals. This bonding situation gives rise to a lowest $\sigma\pi^*$ state whose properties depend strongly on the metal, axial ligand(s) E and E′, and on the solvent. In general, these states are highly reactive. Their population, either by a direct $\sigma \rightarrow \pi^*$ excitation or indirectly via higher ^{1}MLCT states, results in the homolysis of the M–E bond, producing radicals. The rate of this reaction ranges from femtosecond in the case of alkyl or benzyl complexes in polar solvents to 250 ns for Re(Benzyl)$(CO)_3$(*i*Pr-DAB) in toluene or hexane and even to microseconds for Re or Ru complexes containing the strongly bound Ph_3Sn ligand. Bond homolysis is the main deactivation pathway of the $\sigma\pi^*$ states. If the photochemical reaction is suppressed in low temperature glasses or in a non-polar solvent, the $\sigma\pi^*$ states are rather long-lived since their non-radiative decay to the ground state is exceptionally slow. This is caused by the combination of a relatively small excited state distortion with a weak electronic coupling to the ground state. In particular, a very long lifetime was found for the $^3\sigma\pi^*$-excited Ru$(SnPh_3)(CO)_2$(*i*Pr-DAB) whose axial σ orbital is nearly non-bonding and, moreover, largely delocalised over the complex molecule through its mixing with the π^*(diimine) orbital. In general, the large strength of the axial bonds and extended delocalisation of the axial σ electronic density onto the diimine ligand, which may occur both in the ground and excited state, appear to be the most important structural factors which stabilise the $\sigma\pi^*$ state towards both the non-radiative decay and the bond homolysis. The radiative decay is also slow and, hence, the emission from $\sigma\pi^*$ states is rather weak.

Efficient photochemical radical production from Re and Ru carbonyl–diimine complexes with lowest $\sigma\pi^*$ states may find applications in photoinitiation of radical reactions and polymerisations by irradiation with low-energy visible light. Various Mn(E)$(CO)_3$(α-diimine) complexes, whose photoreactivity is similar [55] to that of the Re species, are now being explored as potential photoinitiators [158]. Long intrinsic excited state lifetimes and emissive properties of the $\sigma\pi^*$ states could be exploited in the development of luminophores emissive in red or near-IR spectral regions, should the photoreactivity be suppressed completely. To this effect, osmium complexes with supposedly unreactive $\sigma\pi^*$ excited states are now being developed.

The MLCT, LLCT, or $\sigma\pi^*$ states all involve excitation into the π^*(diimine) orbital. Hence, the properties of a particular excited state are dependent on the structure of the diimine ligand. Structural variations in the diimine ligand present a very promising way to purpose-designed photoactive molecular materials. For

example, a judicious building of delocalisation and rigidity into diimine ligands enables to control excited state lifetimes (almost) independently of the excited state energy [89,91]. The possibility to design complexes with long-lived, relatively low-energy, excited states is especially attractive. Such species would absorb light over most of the visible spectral region and convert the optical energy to the excited state energy that may be further utilised chemically. Diimine complexes may also be linked together [159] through substituents (e.g. $-C\equiv C-$) on the rings of the bpy ligand [160] or by linking together the N donor atoms of the DAB or PyCa ligands by organic spacers [159]. These approaches may lead to photoactive metal-containing polymers. Significant stabilisation of the π^*(diimine) orbital and, hence, a shift of the absorption and emission to the red (or even NIR) spectral region may be accomplished by attaching another metal centre to the potentially bridging ligands like dpp, dpq, bpym. For example, this is the case of trinuclear complexes $Re(Mn(CO)_5)(CO)_3(\mu\text{-L})Re(Br)(CO)_3(bpy)$; L = dpp, bpym; whose irradiation with red light (645 nm) still leads to the Re–Mn bond homolysis from a low-lying $\sigma\pi^*$ state [70,161]. These observations could open a route to photonic materials active under low-energy irradiation. Another important research direction leads to the realm of supramolecular photochemistry and sensors. For example, crown ether units may be attached to the 4,4′ positions of the bpy ligand [17] or to the imine N donor atom of PyCa [15]. DAB and PyCa ligands with long aliphatic substituents on their N atoms form liquid crystalline Re complexes [162,163] whose photophysical properties has not yet been studied. An interesting supramolecular device was formed by linking a bis-anthracene unit to the 3-position of the bpy ligand in $Re(Cl)(CO)_3(bpy)$. Photochemical switching of the former from the monomeric to the dimeric state and vice versa switches the emission of the latter on and off, respectively [164]. A $Re(Cl)(CO)_3$ moiety was also incorporated to large macrocyclic rings containing phen units [165]. Large polycyclic diimine ligands like dppz or dppn, which may form adducts with biomolecules like DNA.

Tuning the properties of the CT states by the structural variations of the diimine ligand is, however, somewhat restricted by the occurrence of low-lying intraligand $\pi\pi^*$ excited states in highly delocalised aromatic diimine ligands. Such an IL state may then become the lowest excited state of the Re(E)(CO)3(α-diimine) molecule, especially if the axial ligand E is a strong π-acceptor and/or if the complex is embedded in a rigid matrix.

6. Conclusions

The character and properties of the lowest excited state of $Re(E)(CO)_3(\alpha\text{-diimine})$ and $Ru(E)(E')(CO)_2(\alpha\text{-diimine})$ complexes can be fine-tuned by variations in the structure of the axial ligand(s), the diimine, or the medium. In general, the lowest excited state can be either of MLCT, LLCT, $\sigma\pi^*$, or IL character. Each of these states has its distinct spectroscopic, photophysical and photochemical properties. The rate of radiative as well as non-radiative decay generally decreases in the order MLCT > LLCT $\gg \sigma\pi^*$. However, the actual lifetime of $\sigma\pi^*$ states may be strongly

diminished by their chemical reactivity. For each type of excited state, a decrease in both radiative and non-radiative decay rate follows the general trend bpy < R-PyCa < R-DAB < Ar-DAB. The Re and Ru carbonyl–diimine complexes are, depending on their structure and environment, promising sensitisers, luminophores, photocatalysts, radical photoinitiators or luminescent probes or sensors. Their potential function depends on the character and properties of their lowest excited state, and, hence, it may be controlled by a judicious choice of the axial and diimine ligands. The understanding of the relations between the structure and excited state properties, together with the great synthetic flexibility of these complexes, opens a way to a rational design of various photonic materials.

Acknowledgements

Mr I.R. Farrell (QMW) is gratefully thanked for his kind help with the manuscript preparation. This work was carried out within the European COST Project D4/0001/94 'Organometallic and Coordination Compounds Capable of Optical Charge-transfer Excitation: Design, Excited State Dynamics, Reactivity and Bistability'.

References

[1] M. Wrighton, D.L. Morse, J. Am. Chem. Soc. 96 (1974) 998.
[2] J.C. Luong, L. Nadjo, M.S. Wrighton, J. Am. Chem. Soc. 100 (1978) 5790.
[3] D.L. Morse, M.S. Wrighton, J. Am. Chem. Soc. 98 (1976) 3931.
[4] G.L. Geoffroy, M.S. Wrighton, Organometallic Photochemistry, Academic Press, New York, 1979.
[5] J.V. Caspar, E.M. Kober, B.P. Sullivan, T.J. Meyer, J. Am. Chem. Soc. 104 (1982) 630.
[6] J.V. Caspar, T.J. Meyer, J. Phys. Chem. 87 (1983) 952.
[7] D.R. Striplin, G.A. Crosby, Chem. Phys. Lett. 221 (1994) 426.
[8] L.A. Worl, R. Duesing, P. Chen, L. Della Ciana, T.J. Meyer, J. Chem. Soc. Dalton Trans. (1991) 849.
[9] E.M. Kober, J.V. Caspar, R.S. Lumpkin, T.J. Meyer, J. Phys. Chem. 90 (1986) 3722.
[10] T.G. Kotch, A.J. Lees, S.J. Fuerniss, K. Papathomas, I.R.W. Snyder, Inorg. Chem. 32 (1993) 2570.
[11] H.D. Stoeffler, N.B. Thornton, S.L. Temkin, K.S. Schanze, J. Am. Chem. Soc. 117 (1995) 7119.
[12] V.W.-W. Yam, K.K.-W. Lo, K.-K. Cheung, R.Y.-C. Kong, J. Chem. Soc. Chem. Commun. (1995) 1191.
[13] V.W.-W. Yam, K.K.-W. Lo, K.-K. Cheung, R.Y.-C. Kong, J. Chem. Soc. Dalton Trans. (1997) 2067.
[14] T.A. Oriskovich, P.S. White, H.H. Thorp, Inorg. Chem. 34 (1995) 1629.
[15] V.W.-W. Yam, K.M.-C. Wong, V.W.-M. Lee, K.K.-W. Lo, K.-K. Cheung, Organometallics 14 (1995) 4034.
[16] L. Sacksteder, M. Lee, J.N. Demas, B.A. DeGraff, J. Am. Chem. Soc. 115 (1993) 8230.
[17] D.I. Yoon, C.A. Berg-Brennan, H. Lu, J.T. Hupp, Inorg. Chem. 31 (1992) 3192.
[18] C.A. Berg-Brennan, D.I. Yoon, R.V. Slone, A.P. Kazala, J.T. Hupp, Inorg. Chem. 35 (1996) 2032.
[19] J.C. Calabrese, W. Tam, Chem. Phys. Lett. 133 (1987) 244.
[20] T.T. Ehler, N. Malmberg, K. Carron, B.P. Sullivan, L.J. Noe, J. Phys. Chem. B. 101 (1997) 3174.

[21] V.W.-W. Yam, V.C.Y.- Lau, K.-K. Cheung, J. Chem. Soc. Chem. Commun. (1995) 259.
[22] K. Kalyanasundaram, J. Chem. Soc. Faraday Trans. 2 (82) (1986) 2401.
[23] W.B. Connick, A.J. Di Bilio, M.G. Hill, J.R. Winkler, H.B. Gray, Inorg. Chim. Acta 240 (1995) 169.
[24] D.M. Roundhill, Photochemistry and Photophysics of Metal Complexes, Plenum Press, New York, 1994.
[25] A. Klein, C. Vogler, W. Kaim, Organometallics 15 (1996) 236.
[26] B.D. Rossenaar, F. Hartl, D.J. Stufkens, Inorg. Chem. 35 (1996) 6194.
[27] G.J. Stor, F. Hartl, J.W.M. van Outersterp, D.J. Stufkens, Organometallics 14 (1995) 1115.
[28] J. Hawecker, J.-M. Lehn, R. Ziessel, Helv. Chim. Acta 69 (1986) 1990.
[29] J. Hawecker, J.-M. Lehn, R. Ziessel, J. Chem. Soc. Chem. Commun. (1983) 536.
[30] C. Kutal, M.A. Weber, G. Ferraudi, D. Geiger, Organometallics 4 (1985) 2161.
[31] C. Kutal, A.J. Corbin, G. Ferraudi, Organometallics 6 (1987) 553.
[32] H. Hori, F.P.A. Johnson, K. Koike, K. Takeuchi, T. Ibusuki, O. Ishitani, J. Chem. Soc. Dalton Trans. (1997) 1019.
[33] F.P.A. Johnson, M.W. George, F. Hartl, J.J. Turner, Organometallics 15 (1996) 3374.
[34] K. Koike, H. Hori, M. Ishizuka, J.R. Westwell, K. Takeuchi, T. Ibusuki, K. Enjouji, H. Konno, K. Sakamoto, O. Ishitani, Organometallics 16 (1997) 5724.
[35] P. Chen, T.D. Westmoreland, E. Danielson, K.S. Schanze, D. Anthon, P.E. Neveux Jr, T.J. Meyer, Inorg. Chem. 26 (1987) 1116.
[36] T.D. Westmoreland, H. Le Bozec, R.W. Murray, T.J. Meyer, J. Am. Chem. Soc. 105 (1983) 5952.
[37] P. Chen, R. Duesing, D.K. Graff, T.J. Meyer, J. Phys. Chem. 95 (1991) 5850.
[38] P. Chen, S.L. Mecklenburg, T.J. Meyer, J. Phys. Chem. 97 (1993) 13126.
[39] J.R. Schoonover, G.F. Strouse, P. Chen, W.D. Bates, T.J. Meyer, Inorg. Chem. 32 (1993) 2618.
[40] N.E. Katz, S.L. Mecklenburg, D.K. Graff, P. Chen, T.J. Meyer, J. Phys. Chem. 98 (1994) 8959.
[41] J.R. Schoonover, P. Chen, W.D. Bates, R.B. Dyer, T.J. Meyer, Inorg. Chem. 33 (1994) 793.
[42] N.E. Katz, S.L. Mecklenburg, T.J. Meyer, Inorg. Chem. 34 (1995) 1282.
[43] G.F. Strouse, J.R. Schoonover, R. Duesing, T.J. Meyer, Inorg. Chem. 34 (1995) 2725.
[44] L.A. Cabana, K.S. Schanze, Adv. Chem. Ser. 226 (1990) 101.
[45] K.S. Schanze, D.B. MacQueen, T.A. Perkins, L.A. Cabana, Coord. Chem. Rev. 122 (1993) 63.
[46] D.J. Stufkens, Comments Inorg. Chem. 13 (1992) 359.
[47] J.P. Claude, D.S. Williams, T.J. Meyer, J. Am. Chem. Soc. 118 (1996) 9782.
[48] Y. Wang, B.T. Hauser, M.M. Rooney, R.D. Burton, K.S. Schanze, J. Am. Chem. Soc. 115 (1993) 5675.
[49] L.A. Lucia, Y. Wang, K. Nafisi, T.L. Netzel, K.S. Schanze, J. Phys. Chem. 99 (1995) 11801.
[50] Y. Wang, L.A. Lucia, K.S. Schanze, J. Phys. Chem. 99 (1995) 1961.
[51] Y. Wang, K.S. Schanze, J. Phys. Chem. 100 (1996) 5408.
[52] S. Trammell, P.A. Goodson, B.P. Sullivan, Inorg. Chem. 35 (1996) 1421.
[53] L.A. Lucia, R.D. Burton, K.S. Schanze, Inorg. Chim. Acta 208 (1993) 103.
[54] B.D. Rossenaar, C.J. Kleverlaan, D.J. Stufkens, A. Oskam, J. Chem. Soc. Chem. Commun. (1994) 63.
[55] B.D. Rossenaar, D.J. Stufkens, A. Oskam, J. Fraanje, K. Goubitz, Inorg. Chim. Acta 247 (1996) 215.
[56] H.A. Nieuwenhuis, M.C.E. van de Ven, D.J. Stufkens, A. Oskam, K. Goubitz, Organometallics 14 (1995) 780.
[57] B.D. Rossenaar, C.J. Kleverlaan, M.C.E. van de Ven, D.J. Stufkens, A. Vlček, Jr., Chem. Eur. J. 2 (1996) 228.
[58] B.D. Rossenaar, M.W. George, F.P.A. Johnson, D.J. Stufkens, J.J. Turner, A. Vlček, Jr., J. Am. Chem. Soc. 117 (1995) 11582.

[59] C.J. Kleverlaan, D.M. Martino, H. van Willigen, D.J. Stufkens, A. Oskam, J. Phys. Chem. 100 (1996) 18607.
[60] C.J. Kleverlaan, D.J. Stufkens, I.P. Clark, M.W. George, J.J. Turner, D.M. Martino, H. van Willigen, A. Vlček, Jr., J. Am. Chem. Soc. 120 (1998) 10871.
[61] C.J. Kleverlaan, D.J. Stufkens, Inorg. Chim. Acta (in press).
[62] J.C. Luong, R.A. Faltynek, M.S. Wrighton, J. Am. Chem. Soc. 102 (1980) 7892.
[63] J.C. Luong, R.A. Faltynek, M.S. Wrighton, J. Am. Chem. Soc. 101 (1979) 1597.
[64] M.W. Kokkes, D.J. Stufkens, A. Oskam, Inorg. Chem. 24 (1985) 4411.
[65] M.W. Kokkes, D.J. Stufkens, A. Oskam, Inorg. Chem. 24 (1985) 2934.
[66] R.R. Andrea, W.G.J. de Lange, T. van der Graaf, M. Rijkhoff, D.J. Stufkens, A. Oskam, Organometallics 7 (1988) 1100.
[67] R.R. Andrea, W.G.J. de Lange, D.J. Stufkens, A. Oskam, Inorg. Chem. 28 (1989) 318.
[68] T. van der Graaf, R.M.J. Hofstra, P.G.M. Schilder, M. Rijkhoff, D.J. Stufkens, J.G.M. van der Linden, Organometallics 10 (1991) 3668.
[69] T. van der Graaf, A. van Rooy, D.J. Stufkens, A. Oskam, Inorg. Chim. Acta 187 (1991) 133.
[70] J.W.M. van Outersterp, D.J. Stufkens, A. Vlček, Jr., Inorg. Chem. 34 (1995) 5183.
[71] H.A. Nieuwenhuis, A. van Loon, M.A. Moraal, D.J. Stufkens, A. Oskam, K. Goubitz, J. Organomet. Chem. 492 (1995) 165.
[72] M.P. Aarnts, D.J. Stufkens, M.P. Wilms, E.J. Baerends, A. Vlček, Jr., I.P. Clark, M.W. George, J.J. Turner, Chem. Eur. J. 2 (1996) 1556.
[73] B.D. Rossenaar, E. Lindsay, D.J. Stufkens, A. Vlček, Jr., Inorg. Chim. Acta 250 (1996) 5.
[74] M.P. Aarnts, M.P. Wilms, D.J. Stufkens, E.J. Baerends, A. Vlček, Jr., Organometallics 16 (1997) 2055.
[75] M.P. Aarnts, D.J. Stufkens, A. Vlček, Jr., Inorg. Chim. Acta 266 (1997) 37.
[76] H.A. Nieuwenhuis, D.J. Stufkens, A. Oskam, Inorg. Chem. 33 (1994) 3212.
[77] H.A. Nieuwenhuis, D.J. Stufkens, A. Oskam, A. Vlček, Jr., Inorg. Chem. 34 (1995) 3879.
[78] H.A. Nieuwenhuis, D.J. Stufkens, R.-A. McNicholl, A.H.R. Al-Obaidi, C.G. Coates, S.E.J. Bell, J.J. McGarvey, J. Westwell, M.W. George, J.J. Turner, J. Am. Chem. Soc. 117 (1995) 5579.
[79] M.P. Aarnts, D.J. Stufkens, A. Oskam, J. Fraanje, K. Goubitz, Inorg. Chim. Acta 256 (1997) 93.
[80] J.W.M. van Outersterp, F. Hartl, D.J. Stufkens, Organometallics 14 (1995) 3303.
[81] R.W. Balk, D.J. Stufkens, A. Oskam, J. Chem. Soc. Dalton Trans. (1981) 1124.
[82] M.P. Aarnts, M.P. Wilms, K. Peelen, J. Fraanje, K. Goubitz, F. Hartl, D.J. Stufkens, E.J. Baerends, A. Vlček, Jr., Inorg. Chem. 35 (1996) 5468.
[83] M.P. Aarnts, A. Oskam, D.J. Stufkens, J. Fraanje, K. Goubitz, N. Veldman, A.L. Spek, J. Organomet. Chem. 531 (1997) 191.
[84] D.J. Stufkens, M.P. Aarnts, B.D. Rossenaar, A. Vlček, Jr., Pure Appl. Chem. 69 (1997) 831.
[85] J.V. Caspar, T.J. Meyer, Inorg. Chem. 22 (1983) 2444.
[86] R.S. Lumpkin, E.M. Kober, L.A. Worl, Z. Murtaza, T.J. Meyer, J. Phys. Chem. 94 (1990) 239.
[87] K.F. Freed, J. Jortner, J. Chem. Phys. 52 (1970) 6272.
[88] R. Englman, J. Jortner, Molec. Phys. 18 (1970) 145.
[89] J.A. Treadway, B. Loeb, R. Lopez, P.A. Anderson, F.R. Keene, T.J. Meyer, Inorg. Chem. 35 (1996) 2242.
[90] G.J. Ferraudi, Elements of Inorganic Photochemistry, Wiley-Interscience, New York, 1988.
[91] G.F. Strouse, J.R. Schoonover, R. Duesing, S. Boyde, W.E. Jones, T.J. Meyer, Inorg. Chem. 34 (1995) 473.
[92] L. Sacksteder, A.P. Zipp, E.A. Brown, J. Streich, J.N. Demas, Inorg. Chem. 29 (1990) 4335.
[93] J.A. Baiano, R.J. Kessler, R.S. Lumpkin, M.J. Munley, W.R. Murphy, Jr., J. Phys. Chem. 99 (1995) 17680.
[94] J.K. Hino, L. Della Ciana, W.J. Dressick, B.P. Sullivan, Inorg. Chem. 31 (1992) 1072.
[95] J.A. Baiano, W.R. Murphy, Jr., Inorg. Chem. 30 (1991) 4594.
[96] S.M. Fredericks, J.C. Luong, M.S. Wrighton, J. Am. Chem. Soc. 101 (1979) 7415.
[97] H. Hori, K. Koike, M. Ishizuka, K. Takeuchi, T. Ibusuki, O. Ishitani, J. Organomet. Chem. 530 (1997) 169.
[98] V.W.-W. Yam, V.C.-Y. Lau, K.-K. Cheung, Organometallics 14 (1995) 2749.

[99] V.W.-W. Yam, V.C.-Y. Lau, K.-K. Cheung, Organometallics 15 (1996) 1740.
[100] R.-J. Lin, K.-S. Lin, I.-J. Chang, Inorg. Chim. Acta 242 (1996) 179.
[101] K. Kalyanasundaram, M. Gratzel, M.K. Nazeeruddin, Inorg. Chem. 31 (1992) 5243.
[102] J.R. Schoonover, K.C. Gordon, R. Argazzi, W.H. Woodruff, K.A. Peterson, C.A. Bignozzi, R.B. Dyer, T.J. Meyer, J. Am. Chem. Soc. 115 (1993) 10996.
[103] C.A. Bignozzi, R. Argazzi, C.G. Garcia, F. Scandola, J. Am. Chem. Soc. 114 (1992) 8727.
[104] G. Tapolsky, R. Duesing, T.J. Meyer, Inorg. Chem. 29 (1990) 2285.
[105] K. Kalyanasundaram, M.K. Nazeeruddin, Inorg Chim. Acta 226 (1994) 213.
[106] R. Lin, T.F. Guarr, Inorg. Chim. Acta 226 (1994) 79.
[107] V. Balzani, A. Juris, M. Venturi, S. Campagna, S. Serroni, Chem. Rev. 96 (1996) 759.
[108] K.M. Omberg, J.R. Schoonover, T.J. Meyer, J. Phys. Chem. A 101 (1997) 9531.
[109] D.J. Stufkens, Coord. Chem. Rev. 104 (1990) 39.
[110] A.J. Lees, Chem. Rev. 87 (1987) 711.
[111] B.D. Rossenaar, D.J. Stufkens, A. Vlček, Jr., Inorg. Chim. Acta 247 (1996) 247.
[112] B.D. Rossenaar, D.J. Stufkens, A. Vlček, Jr., Inorg. Chem. 35 (1996) 2902.
[113] W.K. Smothers, M.S. Wrighton, J. Am. Chem. Soc. 105 (1983) 1067.
[114] R.W. Balk, D.J. Stufkens, A. Oskam, J. Chem. Soc. Dalton Trans. (1982) 275.
[115] D.R. Gamelin, M.W. George, P. Glyn, F.-W. Grevels, F.P.A. Johnson, W. Klotzbucher, S.L. Morrison, G. Russell, K. Schaffner, J.J. Turner, Inorg. Chem. 33 (1994) 3246.
[116] B.D. Rossenaar, C.J. Kleverlaan, M.C.E. van de Ven, D.J. Stufkens, A. Oskam, J. Fraanje, K. Goubitz, J. Organomet. Chem. 493 (1995) 153.
[117] M.W. George, F.P.A. Johnson, J.R. Westwell, P.M. Hodges, J.J. Turner, J. Chem. Soc. Dalton Trans. (1993) 2977.
[118] J.R. Schoonover, G.F. Strouse, R.B. Dyer, W.D. Bates, P. Chen, T.J. Meyer, Inorg. Chem. 35 (1996) 273.
[119] R.J. Shaver, D.P. Rillema, C. Woods, J. Chem. Soc. Chem. Commun. (1990) 179.
[120] R.J. Shaver, D.P. Rillema, Inorg. Chem. 31 (1992) 4101.
[121] G.F. Strouse, H.U. Gudel, V. Bertolasi, V. Ferretti, Inorg. Chem. 34 (1995) 5578.
[122] G.F. Strouse, H.U. Gudel, Inorg. Chim. Acta 240 (1995) 453.
[123] C.J. Kleverlaan, D.J. Stufkens, J. Photochem. Photobiol. A: 116 (1998) 109.
[124] P. Chen, E. Danielson, T.J. Meyer, J. Phys. Chem. 92 (1988) 3708.
[125] R.L. Cleary, K.J. Byrom, D.A. Bardwell, J.C. Jeffery, M.D. Ward, G. Calogero, N. Armaroli, L. Flamigni, F. Barigelletti, Inorg. Chem. 36 (1997) 2601.
[126] V. Balzani, F. Scandola, Supramolecular Photochemistry, Ellis Horwood, Chichester, 1991.
[127] R.J. Shaver, M.W. Perkovic, D.P. Rillema, C. Woods, Inorg. Chem. 34 (1995) 5446.
[128] M.P. Wilms, D.J. Stufkens, E.J. Baerends, A.J. Vlček, Jr., to be published.
[129] G.J. Stor, D.J. Stufkens, P. Vernooijs, E.J. Baerends, J. Fraanje, K. Goubitz, Inorg. Chem. 34 (1995) 1588.
[130] G.J. Stor, D.J. Stufkens, A. Oskam, Inorg. Chem. 31 (1992) 1318.
[131] M.S. Wrighton, J.L. Graff, J.C. Luong, C.L. Reichel, J.L. Robbins, ACS Symp. Ser. 155 (1981) 85.
[132] I.R. Farrell, P. Matovšek A. Vlček, Jr., Inorg. Chem. (in press).
[133] R.R. Andrea, D.J. Stufkens, A. Oskam, J. Organomet. Chem. 290 (1985) 63.
[134] M.P. Wilms, D. Guillaumont, D.J. Stufkens, C. Daniel, Organometallics.
[135] P.E.M. Siegbahn, J. Phys. Chem. 99 (1995) 12723.
[136] M.W. Kokkes, T.L. Snoeck, D.J. Stufkens, A. Oskam, M. Cristophersen, C.H. Stam, J. Molec. Struct. 131 (1985) 11.
[137] R.R. Andrea, W.G.J. de Lange, D.J. Stufkens, A. Oskam, Inorg. Chim. Acta 149 (1988) 77.
[138] D. Guillaumont, C. Daniel, Coord. Chem. Rev. 177 (1998) 181.
[139] D. Guillaumont, K. Finger, M.R. Hachey, C. Daniel, Coord. Chem. Rev. 171 (1998) 439.
[140] J. Reinhold, R. Benedix, P. Birner, H. Hennig, Inorg. Chim. Acta 33 (1979) 209.
[141] P.C. Servaas, H.K. van Dijk, T.L. Snoeck, D.J. Stufkens, A. Oskam, Inorg. Chem. 24 (1985) 4494.
[142] J.R. Schoonover, W.D. Bates, T.J. Meyer, Inorg. Chem. 34 (1995) 6421.
[143] L. Wallace, C. Woods, D.P. Rillema, Inorg. Chem. 34 (1995) 2875.

[144] L. Wallace, D.P. Rillema, Inorg. Chem. 32 (1993) 3836.
[145] P. Glyn, M.W. George, P.M. Hodges, J.J. Turner, J. Chem. Soc. Chem. Commun. (1989) 1655.
[146] M. Feliz, G. Ferraudi, H. Altmiller, J. Phys. Chem. 96 (1992) 257.
[147] N.M. Iha, G. Ferraudi, J. Chem. Soc. Dalton Trans. (1994) 2565.
[148] G. Ferraudi, M. Feliz, E. Wolcan, I. Hsu, S.A. Moya, J. Guerrero, J. Phys. Chem. 99 (1995) 4929.
[149] G. Ruiz, E. Wolcan, M.R. Feliz, J. Photochem. Photobiol. A. 101 (1996) 119.
[150] P.C. Servaas, D.J. Stufkens, A. Oskam, P. Vernooijs, E.J. Baerends, D.J.A. De Ridder, C.H. Stam, Inorg. Chem. 28 (1989) 4104.
[151] P.C. Servaas, W.G.J. De Lange, D.J. Stufkens, A. Oskam, Inorg. Chim. Acta 173 (1990) 175.
[152] F. Hartl, A. Vlček, Jr., Inorg. Chem. 35 (1996) 1257.
[153] F. Hartl, A. Vlček, Jr., D.J. Stufkens, Inorg. Chim. Acta 192 (1992) 25.
[154] F. Hartl, A. Vlček, Jr., Inorg. Chem. 31 (1992) 2869.
[155] M. Maestri, V. Balzani, C. Deuschel-Cornioley, A. von Zelewsky, in: D. Volman, G. Hammond, D. Neckers (Eds.), Advances in Photochemistry, vol. 17, Wiley, New York, 1992.
[156] F.W.M. Vanhelmont, G.F. Strouse, H.U. Gudel, A.C. Stuckl, H.W. Schmalle, J. Phys. Chem. 101 (1997) 2946.
[157] F.W.M. Vanhelmont, H.U. Gudel, M. Fortsch, H.-B. Burgi, Inorg. Chem. 36 (1997) 5512.
[158] M.P. Aarnts, D.J. Stufkens, to be published.
[159] I.S. Calonaci, J.H. van't Hoff Research Institute, Universitat van Amsterdam, The Netherlands, 1995.
[160] K.D. Ley, C.E. Whittle, M.D. Bartberger, K.S. Schanze, J. Am. Chem. Soc. 119 (1997) 3423.
[161] J.W.M. van Outersterp, D.J. Stufkens, J. Fraanje, K. Goubitz, A. Vlček, Jr., Inorg. Chem. 34 (1995) 4756.
[162] S. Morrone, G. Harrison, D.W. Bruce, Adv. Mater. 7 (1995) 665.
[163] S. Morrone, D. Guillon, D.W. Bruce, Inorg. Chem. 35 (1996) 7041.
[164] A. Beyeler, P. Belser, L. De Cola, Angew. Chem. Int. Ed. Engl. 36 (1997) 2779.
[165] J.-M. Kern, J.-P. Sauvage, J.-L. Weidmann, N. Armaroli, L. Flamigni, P. Ceroni, V. Balzani, Inorg. Chem. 36 (1997) 5329.